EFFECTS OF THREE CARDIOMYOPATHIC-CAUSING

MUTATIONS (D230N, D84N, AND E62Q) ON THE STRUCTURE AND

FLEXIBILITY OF α-TROPOMYOSIN

By

Teryn A. Holeman

A Thesis Submitted to the Faculty of the

GRADUATE INTERDISIPLINARY PROGRAM IN PHYSIOLOGICAL

SCIENCES

In Partial Fulfillment of the Requirements

For the Degree of

MASTER OF SCIENCE

In the Graduate College

THE UNIVERSITY OF ARIZONA

2017

STATEMENT BY AUTHOR

The thesis titled *Effects of Three Cardiomyopathic-Causing Mutations (D230N, D84N, and E62Q) on the Structure and Flexibility of α-Tropomyosin* prepared by Teryn Holeman has been submitted in partial fulfillment of requirements for a master's degree at the University of Arizona and is deposited in the University Library to be made available to borrowers under rules of the Library.

Brief quotations from this thesis are allowable without special permission, provided that an accurate acknowledgement of the source is made. Requests for permission for extended quotation from or reproduction of this manuscript in whole or in part may be granted by the copyright holder.

SIGNED: Teryn Holeman

APPROVAL BY THESIS DIRECTOR

This thesis has been approved on the date shown below:

_____   *May 3rd, 2017*

Jil C. Tardiff M.D., Ph.D.   *Defense Date*

Professor of Cellular and Molecular Medicine

Stephen M. Gootter Endowed Chair

Acknowledgements

First, I would like to thank my mentor, Dr. Jil C. Tardiff for welcoming me as her first Masters student. You have helped me develop my skills as a scientist and have challenged me intellectually. I would also like to thank my committee: Dr. Henk Granzier and Dr. John Konhilas for your valuable insight and guidance this year. I appreciate your continued support as I continue to pursue my dreams as a physician scientist.

I cannot express my love and appreciation to the Tardiff lab members for your support every step of this process. Melissa Lynn, you have been a wonderful mentor and teacher in life and at the benchtop. I can only aspire to someday have the confidence and knowledge that you exude daily. It was amazing sharing several projects with you and life experiences along the way, but I know that this isn't the end :]. Sarah Lehman, you are the most self-less and caring person I have ever met. You are not only intelligent and a hard worker, but you are genuine and have never hesitated to help when I needed you most. I could not have done it without you. Mark McConnell, thank you for the countless hours that you have spent teaching and troubleshooting this year. Also, a huge shout out to Matthew Klass, Mandy Richards, and Grace Benitez for the wonderful memories!

Ultimately, this would not have been possible without my friends, family, and wonderful fiancé. Alex Huhn, I honestly wouldn't be the person I am today without your understanding, love, and unwavering support. To the friends and family that have been on this journey with me, thank you for your understanding, love, and kindness.

Finally, thank you to the animals that gave their lives for my research.

Table of Contents

List of Figures

List of Tables

Abstract

Cardiac contraction at the level of the sarcomere is regulated by the thin filament (TF) composed of actin, alpha tropomyosin (TPM), and the troponin (Tn) complex (cTnT: cTnC: cTnI). The "gate-keeper" protein, α-TPM, is a highly conserved α-helical, coiled-coil dimer that spans actin and regulates myosin-actin interactions. The N-terminus of one α-TPM dimer inter-digitates with the C-terminus of the adjacent dimer in a head-to-tail fashion forming the flexible and cooperative TPM-overlap that is necessary for myofilament activation. Two dilated cardiomyopathy (DCM) causing mutations in TPM (D84N and D230N) and one hypertrophic cardiomyopathy (HCM) causing mutation (E62Q), all identified in large, unrelated, multigenerational families, were utilized to study how primary alterations in protein structure cause functional deficits. We hypothesize that structural changes from a single point mutation propagate along the α-helical coiled-coil of TPM, thus affecting its regulatory function. Structural effects of the mutations studied via differential scanning calorimetry (DSC) on TPM alone revealed significant changes in the thermal unfolding temperatures of both the C- and N-termini for all mutants compared to WT, indicating that mutational effects propagate to both ends of TPM, thus affecting the overlap region. Although, of note, the proximal termini to the mutation has shown more significant structural changes compared to WT. DSC

analysis on fully reconstituted TF's (Tn:TPM:Actin) revealed effects on the TPM-Actin cooperativity of activation, affecting interaction strength (thermal stability), and the rigidity of TPM moving along actin (FWHM). To characterize the resultant functional effect of these discrete changes in thermal stability and TPM rigidity, ATPase assays were used to measure actomyosin activation in the presence and absence of Ca^{2+}. Together, these data will provide a molecular level understanding of the structural and functional deficits caused by these mutations to help elucidate the mechanisms leading to disease.

Introduction

Cardiomyopathies

In the 1980's the World Health Organization classified cardiomyopathies as "heart muscle diseases of unknown cause" [1]. It quickly became evident that this definition was not sufficient to describe the complex heterogeneity with which these diseases present. Today, the American Heart Association (AHA) defines cardiomyopathies as a heterogeneous group of diseases in the myocardium that are attributed to a variety of causes, most frequently genetic, and often lead to cardiovascular death [2]. Individual progression of disease is unique to each patient, but usually presents with ventricular remodeling. However, the structure to function relationships have still not been established.

As more distinguishing characteristics within these cardiomyopathies became clearer, more specific classifications evolved. As of 2016, the AHA recognizes 6 subsets of cardiomyopathies, including Dilated Cardiomyopathy (DCM) and Hypertrophic Cardiomyopathy (HCM). DCM is typically characterized by an increase in chamber size and thinning of the ventricular wall, and causes systolic failure due to reduced ejection fractions (<40%) [3]. It is the most common cause of heart failure and represents the most frequent reason for heart transplantation [3].

HCM is the leading cause of sudden cardiac death in people under 35 and is typically characterized by an asymmetric thickening of the septum and ventricular wall accompanied by a decrease in left ventricular chamber size. In these patients, systolic performance is preserved, while relaxation is impaired, resulting in inadequate filling of the heart. HCM was initially described in the 1950s by Teare as sudden death and asymmetrical hypertrophy in young adults [5]. However, several decades later, the Seidman laboratory showed that a mutation, R403Q in human β-myosin heavy chain (β-MyHC) was causative of HCM [4], linking a genetic insult with the disease for the first time. Since, over 100 single amino acid deletions, substitutions, and additions have been identified within the sarcomere and are known to give rise to a variety of cardiomyopathies, including HCM and DCM. It is estimated that as much as 30% of genetic DCM (affecting 1/2500 people globally) and nearly all genetic hypertrophic cardiomyopathy (HCM) (affecting 1/500 people globally) is a result of mutations in sarcomeric proteins [4]. While the end stages of these progressive diseases are well documented, the initial stages, before apparent clinical symptoms and denoted genotype-positive, phenotype-negative, are poorly understood.

The Cardiac Sarcomere

The cardiac sarcomere is the fundamental unit of contraction in the heart and is made up primarily of thin filaments and thick filaments. The regulatory thin filament is primarily made up of five proteins, filamentous actin, tropomyosin (TPM), and troponin (Tn) complex (C, T, I), that when complexed, regulate contraction and relaxation (Figure 1). The thin filament's F-actin is a formed as a double helical strand of polymerized G-actin monomers [8]. Tn is composed of three subunits: troponin T (TnT) keeps the complex anchored to TPM, troponin I (TnI) inhibits actomyosin activation, and troponin C (TnC) which acts as the calcium sensor [9]. The thick filament comprised of mostly myosin, the "motor protein" of the sarcomere. Through an ATP-dependent process termed cross-bridge cycling, the thin and thick filaments interact and slide along each other, forming the force-generating cross-bridges that result in cardiac contraction.

Tropomyosin Structure and Cooperativity

TPM is the canonical alpha helical coiled coil protein [11,12]. In the human heart, the predominant form is alpha-tropomyosin, a 284-amino acid protein, which forms a dimer. Each tropomyosin (TPM) monomer is comprised of a seven-heptad repeat (positions a-g, Figure 2). Residues in positions "a" and "d" are typically hydrophobic and make up the core of the coiled coil dimer. Residue positions "e" and "g" are typically salt bridges and further stabilize the interaction of the two monomers of TPM. Residues in positions "b", "c", and "g" are solvent exposed and available for interactions with other proteins including actin and the Tn complex, giving it the ability to rapidly transmit regulatory status throughout the thin filament.

Each TPM dimer is associated with one functional unit of the thin filament, including one troponin complex, and seven F-actin monomers (Figure 1). TPM can interact with each of the seven globular units within polymerized F-actin at specific residues, contouring its shape to wrap around the actin filaments. To maximize interactions with actin, inter-protein linkage of adjacent TPM dimers is necessary to form a continuous cable along the entire length of the thin filament [13,14]. Furthermore, this overlap region of TPM is also a region of TPM-Tn interactions and thus is critical to overall function of the sarcomere [15,16].

Figure 1: *Atomistic model (Schwartz et al.) of the cardiac thin filament and regulatory proteins. The thin filament is composed of actin shown in grey, tropomyosin in orange and green (TPM) and the troponin complex: TnI is presented in blue, TnC in red, TnT is in yellow. The C-terminal of one TPM in shown in orange and the N-terminal of the adjacent TPM in green. The enlargement demonstrates the structure of the TPM overlap region. Model image courtesy of Michael R. Williams, Schwartz group, University of Arizona.*
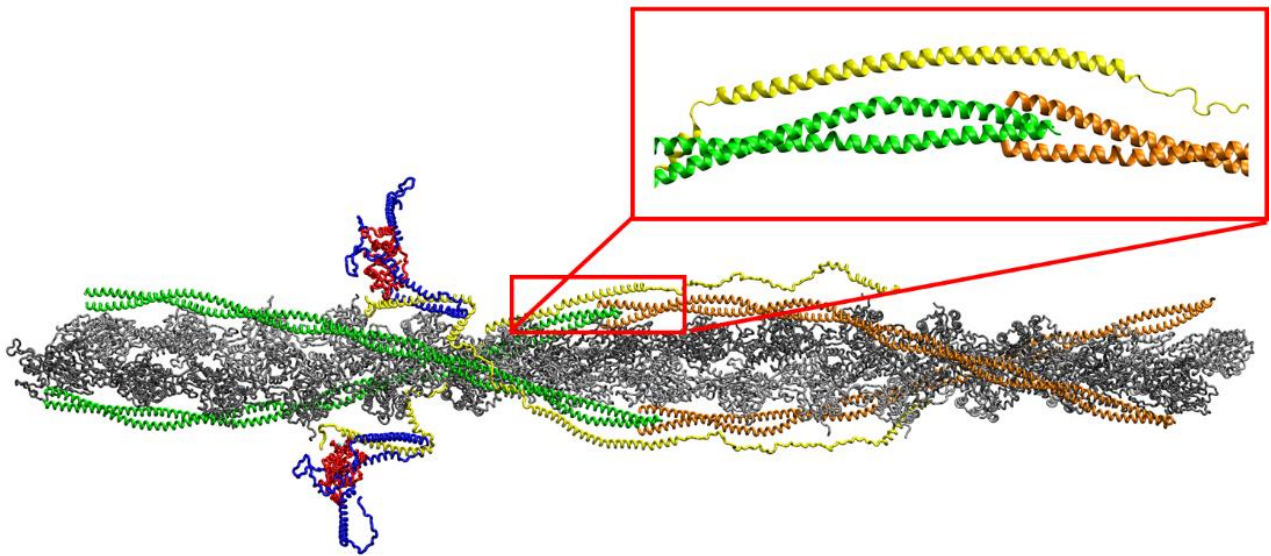
Figure 2: *Atomistic model (Schwartz et al.) of a single TPM dimer (top) with mutant locations indicated: D230N in red, D84N in green, and E62Q in light blue. The C- and N- termini are labeled. α-helical wheel (bottom): cross section representation of a coiled coil TPM dimer showing the heptad repeats of each TPM. Heptad repeats are labeled a→g and a'→g' on each of the two helices, where a and d are hydrophobic residues, e and g are acidic or basic residues and b, c, and f are surface residues [17]. The D230N and E62Q mutation lie within the "f" position and the D84N mutation lies within the "g" position.*

C-Terminus   N-Terminus
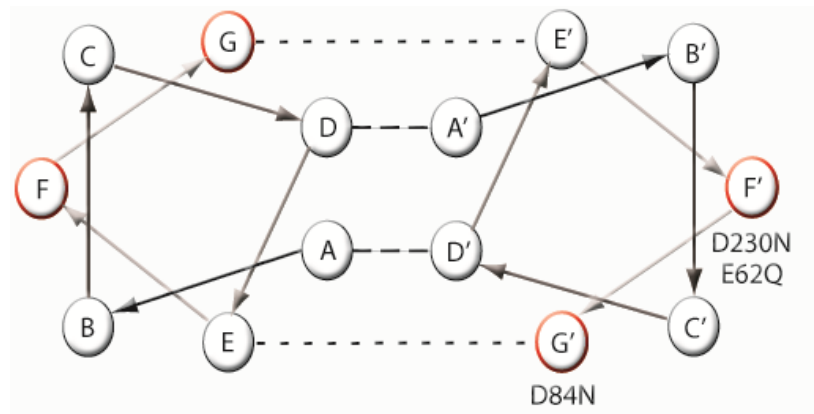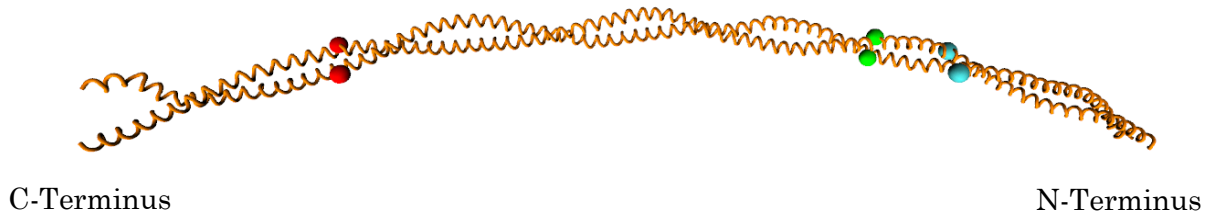
Cooperativity of TPM dimers to shift and move together along actin as one system requires communication between adjacent TPM dimers at the overlap region (Figure 1, enlargement). The N-terminus of one α-TPM dimer inter-digitates with the C-terminus of the adjacent dimer in a head-to-tail fashion forming the flexible and continuous filament [6,18]. The many weak electrostatic interactions that occur along TPM's length with actin are stabilized by the overlap of adjacent TPM dimers. This region is further stabilized by interactions with the N-terminus of troponin T (TnT), which support the dynamic range of motion along actin necessary for the regulation of cross bridge cycling (Figure 1, enlargement (yellow)) [15]. The stability conferred on TPM via TnT and many weak electrostatic interactions with actin are paramount to its regulatory function, while also maintaining the intrinsic flexibility as it must be able to rotate substantially around actin to modulate its position based on the status of the system [19, 20]. The specificity of these interactions make it unsurprising that a mutation in TPM could have a profound impact on its association with actin and TnT and therefore its ability to regulate contraction, resulting in pathology [21].

Cross bridge Cycling and the Three State Model

The actomyosin "gatekeeper" TPM plays a critical role in regulating cross-bridge cycling via its average position of TPM on the surface of actin. This "three-state" model of TPM is described by the blocked, closed, and open states which are modulated by intracellular Ca^{2+} concentrations and myosin (Figure 3) [22-24]. A cross bridge cycle begins with ATP binding to a rigor-bound myosin head attached to the actin filament. ATP binding allows the myosin head to detach from actin and is no longer contributing to force generation. When ATP is hydrolyzed into ADP and an inorganic phosphate ion (Pi), myosin undergoes a conformational change that exposes the actin binding sites on myosin, priming the heads to weakly bind to actin. However, there is no calcium present in the system at this time, so the Tn complex holds TPM in a blocked position that maximally hinders actomyosin activation. Once activation is initiated, calcium-induced-calcium-release raises intracellular calcium levels to a level sufficient for contraction. TnC binds the free calcium and through a series of allosteric protein-protein interactions within the troponin complex, TPM movement from the "blocked" position and into the "closed" position is initiated, leading to the exposure of weak myosin binding sites on actin (Figure 3). The formation of many weak cross bridges cooperatively shift the TPM on actin from the "closed" to the "open" state, resulting in an exposure of the strong-binding myosin sites and a fully-

activated cross-bridge. The power stroke occurs as the inorganic phosphate (P_i) leaves the ATP binding pocket and the thick and thin filaments slide past each other. Myosin releases ADP and is maintained in the rigor position until it binds another ATP molecule. Of note, each of the regulatory TPM positions is an equilibrium between all three average states of TPM on actin and changes to the system just bias the equilibrium is the corresponding direction.

Figure 3: *The three-state model of TPM equilibrium that regulates myofilament activation. The blocked state has minimal binding of the myosin head (S1). Upon addition of calcium, TPM shifts on the surface to the closed state. In this position, the weak binding sites on actin are exposed. Myosin can then bind to actin, and further shift TPM to the open state. This fully activated state requires both calcium and myosin. The corresponding positions are shown on the atomistic model of the thin filament (bottom).*

Figure from Manning et. al, Biophys J. Aug 30; 50(34): 7405-7413.

blocked ↔ closed ↔ open

$-Ca^{2+}$ $+Ca^{2+}$ $+Ca^{2+}$

myosin detached   myosin weakly   myosin strongly
from actin   bound to actin   bound to actin

(no force generation)   (no force generation)   (force generation, crossbridge cycling)
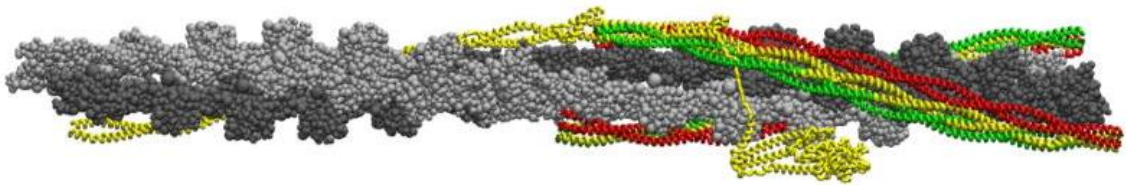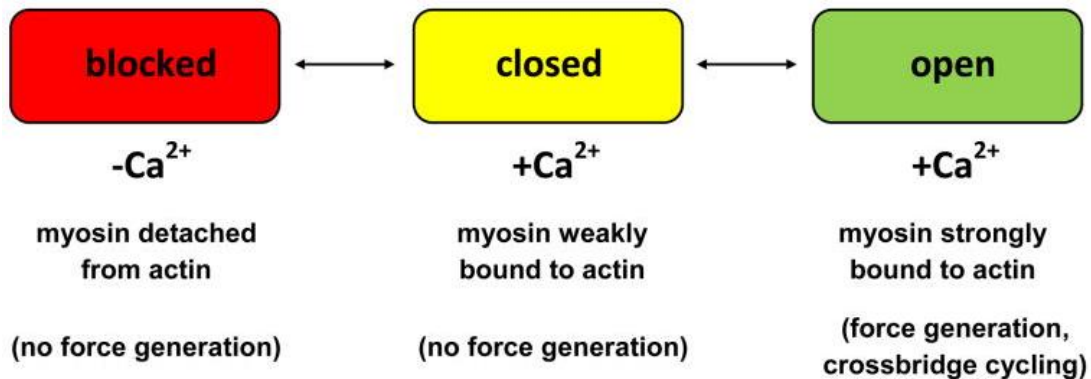
Tropomyosin Mutations Investigated

Since the discovery of the first mutation in a sarcomeric protein (β-myosin), greater than 100 mutations in sarcomeric proteins have been implicated in the development of HCM and DCM [25]. In this thesis, three mutations were chosen within α-TPM due to similarities in phenotype, primary structure, and position on the helix (Figure 2) to elucidate mechanistic pathways leading to disease. Two DCM causing mutations in TPM (D84N and D230N) and one HCM causing mutation (E62Q), all identified in large, unrelated, multigenerational families, were utilized to study how primary alterations in TPM structure cause functional deficits.

The D230N-TPM mutation was first identified in 2010 in two large unrelated mutigenerational families and found to be causative for DCM [26]. The mutation results in a negative charge loss (Aspartic acid to Asparagine) at a solvent exposed residue (f-position), in the 6th period of tropomyosin, proximal to the TPM C-terminus (Figure 2). Affected family members exhibited reduced ejection fraction and enlargement of the left ventricle with a high degree of penetrance (80%). The D84N-TPM mutation is also a negative charge loss mutation, substituting an Aspartic acid to an Asparagine, and causative of DCM [3]. It lies within the "g" position of the helical wheel, stabilizing salt bridge formations within the 2nd period of tropomyosin (Figure 2). The mutation presented in a large, four-generational family with a 90%

23

penetrance and functional deficits including a reduced ejection fraction. The most N-terminus proximal mutation, E62Q-TPM is a substitution of Glutamine for a Glutamic acid resulting in a negative charge loss. E62Q lies within the 2nd period of TPM, in an external "f" position that is known to interact with actin. E62Q is HCM-causative and presented in a large, five-generation family with sepal thickness >13 mm and 75% penetrance [27].

Aims of the Project

The regulatory function of the thin filament over a wide range of physiological demands depends on its ability to transmit seemingly small signals to distant portions of the multi-protein structure via allostery. As our laboratory and others have previously shown, mutations in thin filament proteins can cause allosteric effects that alter the structure of a protein at sites "at a distance" from the actual mutation [28,29]. We hypothesize that structural changes from a single point mutation within TPM can propagate along the α-helical coiled-coil of TPM, thus affecting its regulatory function via the crucial TPM overlap.

The goal of this project is to identify mechanistic patterns of a hypertrophic and dilated cardiomyopathies. Although genetic basis of hypertrophic cardiomyopathy and dilated cardiomyopathy is widely recognized, our understanding of the precise mechanisms underlying the disease remain unclear. Over the last three decades there has been a marked decline in the innovation of cardiovascular pharmaceuticals owed partially to the vast complexity of disease presentation and progression [3]. In addition, we are only clinically able to treat the end stages of disease. By the time patients become symptomatic, the pathological remodeling is usually not reversible and therapeutics are primarily used for symptom palliation. Mechanistic links are necessary to understanding the structural and

25

functional deficits caused by these mutations for improved management of disease. Mechanistic links are necessary to understanding the structural and functional deficits caused by these mutations for better amelioration of disease.

Results

Mutational Effects on Tropomyosin Structure

To study the mutational impact on the secondary structure and thermal stability of WT and D230N-TPM, circular dichroism (CD) was performed by Melissa Lynn, a graduate student in the Tardiff laboratory. These results showed no statistical difference in the helicity between D230N and WT-TPM, as they were both nearly 100% alpha helical (Figure 4, inset). CD was then used to assess the thermal stability of D230N-TPM by plotting the residual ellipticity at 222 nm as a function of temperature. The thermal stability was dependent on the unfolding temperature (T_m). D230N-TPM significantly increased the T_m compared to WT (D230N T_m: 45.4 ± 0.1 °C; WT T_m: 44.2 ± 0.1 °C) (Figure 4, Table 1). This increase in thermal stability indicates a decreased flexibility for a D230N-TPM monomer compared to WT-TPM.

The mutational alterations in tropomyosin tertiary structure were examined using Differential Scanning Calorimetry (DSC). DSC measures the energy input required to denature the protein as a function of temperature with respect to a reference cell filled with buffer. DSC is sensitive enough to separate and characterize both calorimetric domains of TPM unfolding that correspond to the C- and N-terminus respectively. This provides regional data on how perturbations propagate through the TPM dimer [21,30]. D230N-TPM

27

Figure 4: *Thermal stability and structure of human WT and D230N-TPM assessed via CD. The mean residue ellipticity of 0.3 mg/mL WT (blue) and D230N (red) at 222 nm is graphed as a function of temperature. The EC_{50} of these curves yielded melting temperatures (T_m) for WT (44.0 ± 0.1°C) and D230N-TPM (45.3 ± 0.1°C). Inset: Wavelength scan from 200 to 260 nm of WT and D230N-TPM at 20°C. n=3, each an average of 3-5 scans.*
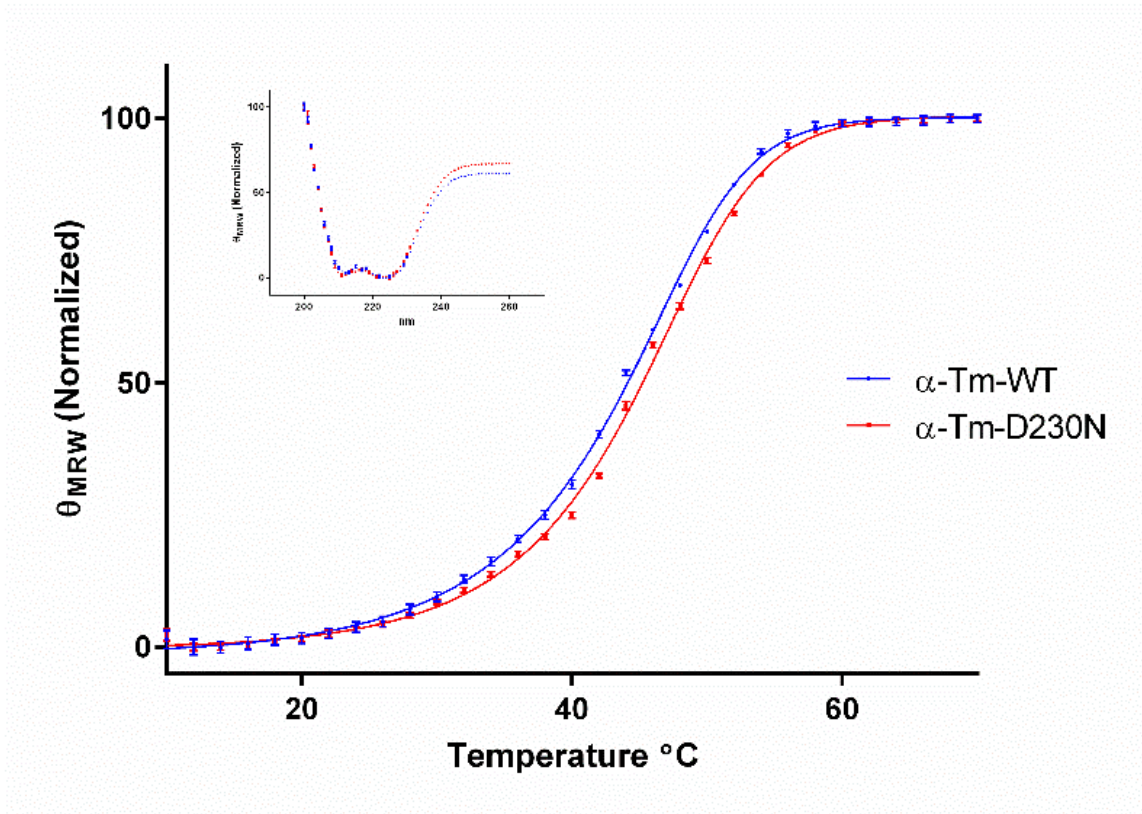
Table 1: *Summary of unfolding temperature from CD (Figure 4) of WT-TPM and D230N-TPM. Values of T_m are expressed as mean S.E.M. Extra sum of squares F test and least squares fit analysis were used for statistical comparison of WT to D230N-TPM. **** $p < 0.0001$.*

Circular Dichroism: Thermal Unfolding	
	T_m °C
α-TPM-WT	44.2 ± 0.1
α-TPM-D230N	45.4 ± 0.1 ****

exhibited significantly increased thermal stability for the C- and N- termini (D1 and D2, respectively) compared to WT- TPM, (D230N-TPM, D1: 44.7 ± 0.02 °C, D2: 52.1 ± 0.02 °C; WT-TPM, D1: 43.9 ± 0.05 °C, D2: 51.6 ± 0.05 °C) as seen by a rightward shift in the peak T_m value of each domain (Figure 5, Table 2). This is consistent with the CD results of a single monomer, indicating a decrease in the D230N-TPM flexibility.

Both DCM-causative mutations, D230N and D84N, had opposing effects on the C- terminus, with D84N-TPM showing a significant decrease in the unfolding temperature of the C-terminus. They both, however, led to stabilization of the N-terminus with a substantial increase in T_m (D84N-TPM, D1: 40.7 ± 0.02 °C, D2: 53.8 ± 0.04 °C; WT-TPM, D1: 43.9 ± 0.05 °C, D2: 51.6 ± 0.05 °C) (Figure 6, Table 2). Of note, these shifts were more pronounced in the D84N-TPM for both termini (>2 °C). The HCM-causative mutation, E62Q, showed shifts in the same direction as the D84N mutation, destabilizing the C-terminus, while increasing the thermal stability of the N-terminus (E62Q-TPM, D1: 43.0 ± 0.01 °C, D2: 54.1 ± 0.04 °C; WT-TPM, D1: 43.9 ± 0.05 °C, D2: 51.6 ± 0.05 °C) (Figure 7, Table 2).

DSC also measures the enthalpy (ΔH) of unfolding that results from heat-induced denaturation and can elucidate factors that contribute to folding and stability. For the WT-TPM samples, the total energy is 9.8 ± 0.18 J/g and the percent enthalpy in each unfolding event is similar, 4.1 ± 0.07 J/g (42%) for

Table 2: *Summary of regional calorimetric data obtained from DSC of WT-TPM, D230N-TPM, D84N-TPM, and E62Q-TPM. The thermal unfolding temperature at the peak maximum is denoted by T_m (°C). Total calorimetric enthalpy was measured and percent (%) of total enthalpy at each terminal was calculated. The values are reported as mean ± S.E.M. One-way ANOVA was used to determine statistical significance. for all mutant T_m values compared to WT, ****$p < 0.0001$ *** $p < 0.001$, * $p < 0.05$.*

DSC- Tm Dimer					
		Domain-1 (C-terminus)		Domain-2 (N-terminus)	
	Total ΔH (J/g)	T_m °C	ΔH J/g (% total)	T_m °C	ΔH J/g (% total)
WT-Tm	9.8 ± 0.18	43.9 ± 0.05	4.1 ± 0.07 (42%)	51.6 ± 0.05****	5.7 ± .22 (58%)****
D230N-Tm	13.4 ± 0.03****	44.7 ± 0.02****	7.3 ± 0.13 (54%)****	52.1 ± 0.02****	6.1 ± 0.07 (46%)****
D84N-Tm	11.4 ± 0.16***	40.7 ± 0.02****	2.4 ± 0.12 (21%)****	53.8 ± 0.04****	9.0 ± 0.06 (79%)****
E62Q-Tm	9.0 ± 0.02*	43.0 ± 0.01****	1.5 ± 0.04 (16%)****	54.1 ± 0.04****	7.7 ± 0.06 (84%)****

Figure 5: *Thermal Stability of WT and D230N-TPM assessed via DSC. The calorimetric enthalpy (J/g*K) of WT (blue) and D230N (red) TPM is graphed as a function of temperature. Two calorimetric domains are seen in the TPM-dimer corresponding to the C- (D1) and N-terminus (D2). D230N-TPM shows a rightward shift in the peak maxima for both unfolding events. These are representative images after subtraction of baseline and instrumental background. The concentration of fully reduced protein of both samples was 1.8 mg/mL. The heating rate was 1°C/min from 25-75°C (n=3). Reported values were determined from the fit of two Gaussian curves.*
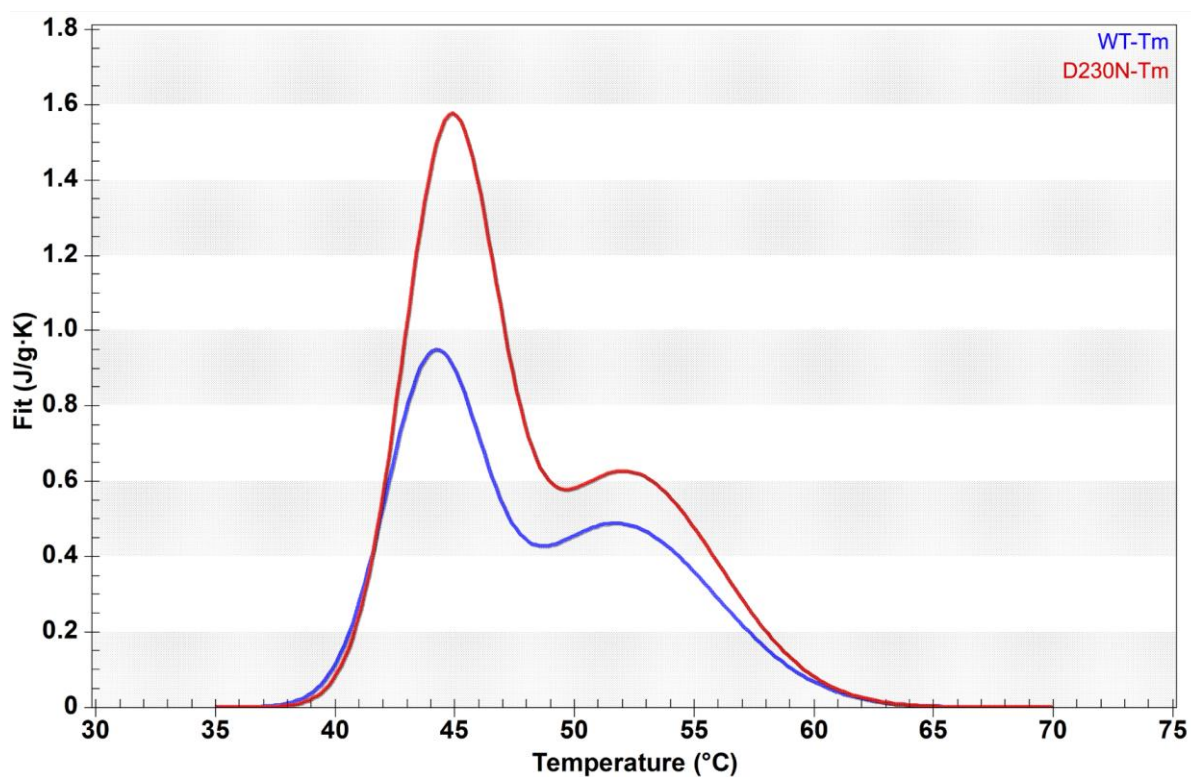
Figure 6: *Thermal Stability of WT and D84N-TPM assessed via DSC. The heat capacity (J/g*K) of WT (blue) and D84N (green) TPM is graphed as a function of temperature. D84N-TPM shifts the D1 to the left, and D2 to the right. These are representative images after subtraction of baseline and instrumental background. The concentration of fully reduced protein of both samples was 1.8 mg/mL. The heating rate was 1°C/min from 25-75°C (n=3). Reported values were determined from the fit of two Gaussian curves.*
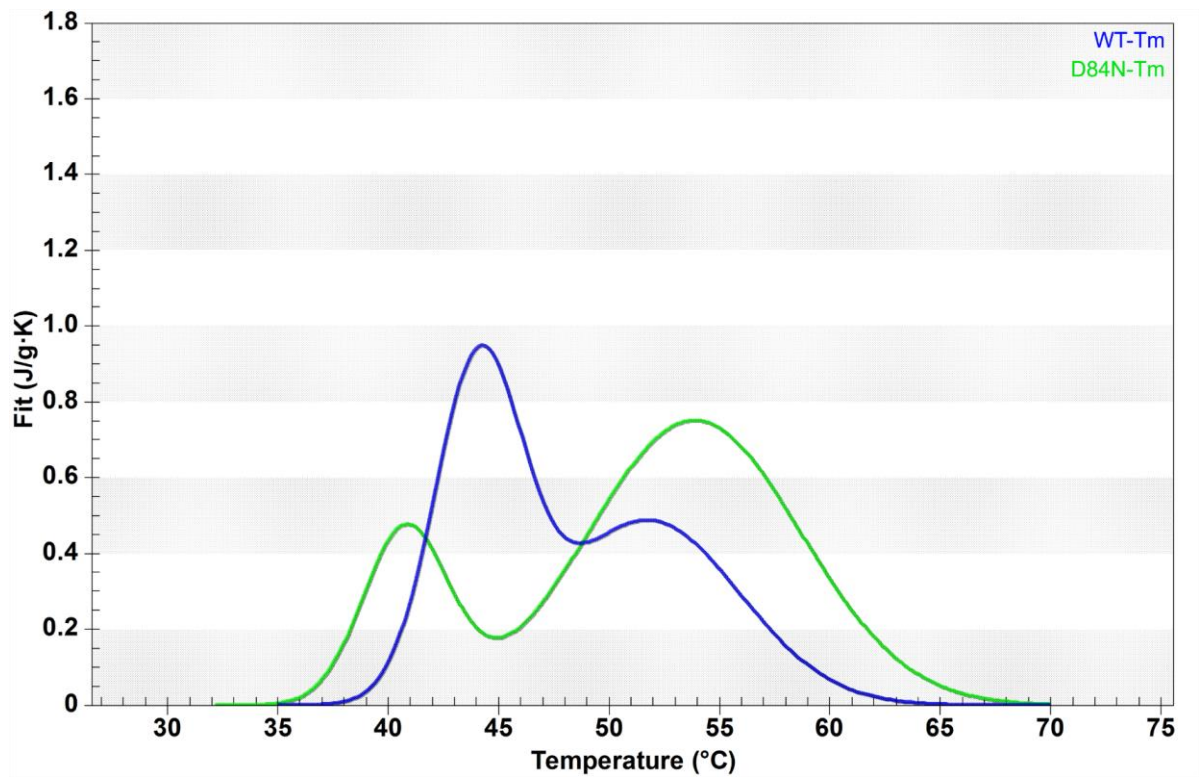
Figure 7: Thermal Stability of WT and E62Q-TPM assessed via DSC. The heat capacity (J/g*K) of WT (blue) and E62Q (cyan) TPM is graphed as a function of temperature. E62Q-TPM shows destabilization of the first domain and stabilization of the second domain. These are representative images after subtraction of baseline and instrumental background. The concentration of fully reduced protein of both samples was 1.8 mg/mL. The heating rate was 1°C/min from 25-75°C (n=3). Reported values were determined from the fit of two Gaussian curves.
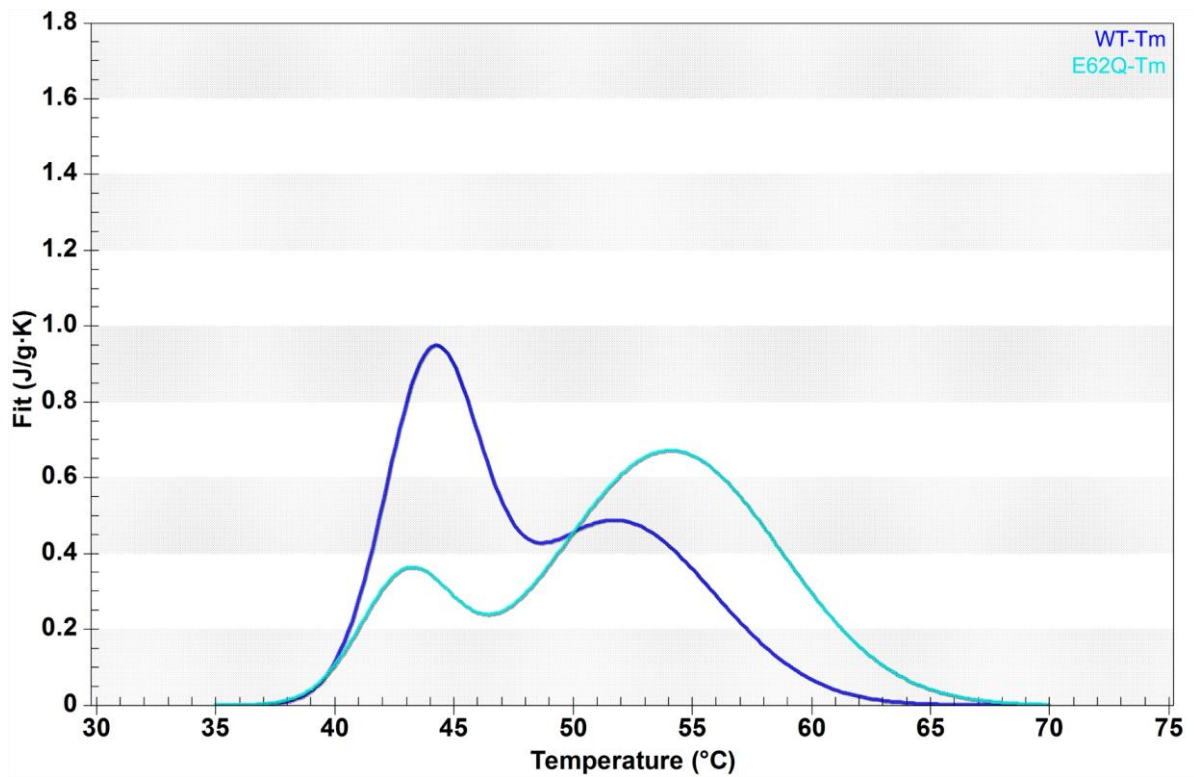
the first event (D1) and 5.7 ± .22 J/g (58%) for the second event (D2). D230N-TPM increases the total enthalpy to 13.4 ± 0.03 J/g (Table 2). The replacement of the asparagine for the aspartic acid residue shifts the enthalpy to 7.3 ± 0.13 J/g (54%) for the C-term (D1) and 6.1 ± 0.07 J/g (46%) for the second domain (D2), altering the enthalpy distribution (Figure 5, Table 2). This phenomenon is described by Gibb's free energy equation: $\Delta G = \Delta H - T\Delta S$ [31]. At the peak maximum, the system is at equilibrium and the Gibbs free energy is constant as it undergoes the transition to denaturation. The D230N-TPM mutation increases the enthalpy of unfolding for both domains, paralleled by an increase in thermal stability of both termini as well. This causes a decrease in entropy (ΔS), indicating that the system has become less disordered, or more rigid.

D84N, like D230N, increases the total calorimetric enthalpy required to unfold the protein to 11.4 ± 0.16 J/g (WT-TPM: 9.8 ± 0.18 J/g), and biases the energy distribution to the terminus proximal to the mutation. The D84N-TPM energy distribution shifted towards the N -terminus {D84N-TPM D1 2.4 ± 0.12 J/g (21%), D2 to 9.0 ± 0.06 J/g (79%); WT-TPM D1, 4.1 ± 0.07 J/g (42%), D2 5.7 ± .22 J/g (58%)} (Figure 6, Table 2). The total enthalpy (ΔH_{cal}) for E62Q mutant was less than WT-TPM (E62Q-TPM: 9.0 ± 0.02 J/g; WT-TPM: 9.8 ± 0.18 J/g) and more energy was required to unfold the proximal N-terminus (1.5 ± 0.04 J/g (16%) for the C-terminus and 7.7 ± 0.06 J/g (84%) for the N-terminus) (Figure 7, Table 2).

Of note, all mutations affected both termini, regardless of the alpha-helical position and period in TPM. This suggests that the mutational effects of a single amino acid substitution can be propagated a significant distance. This is supported by MD simulations performed by Mike Williams and Lukasz Szatkowski, our collaborators in the Schwartz laboratory. The fully solvated, all atom model of the regulatory thin filament showed D230N-TPM decreases the root mean square fluctuation (RMSF) values at both termini compared to WT, corresponding to a decrease in flexibility (Figure 8). These results may indicate that the structural deficits caused by these mutations are transmitting to both termini, potentially affecting the cooperativity TPM-TPM overlap region and myofilament activation.

Figure 8: *RMSF VMD plugin was used to generate RMSF plots for each separate trajectory on the all atom model of the thin filament. RMSF values represent how carbons alpha of each residue are mobile during a trajectory with respect to TPM position. A bigger RMSF value means that this residue moves more during trajectory. Arithmetic average values (from 3 trajectories) were calculated for each residue for WT and D230N. Image courtesy of Lukasz Szatkowski in the Schwartz group, University of Arizona.*
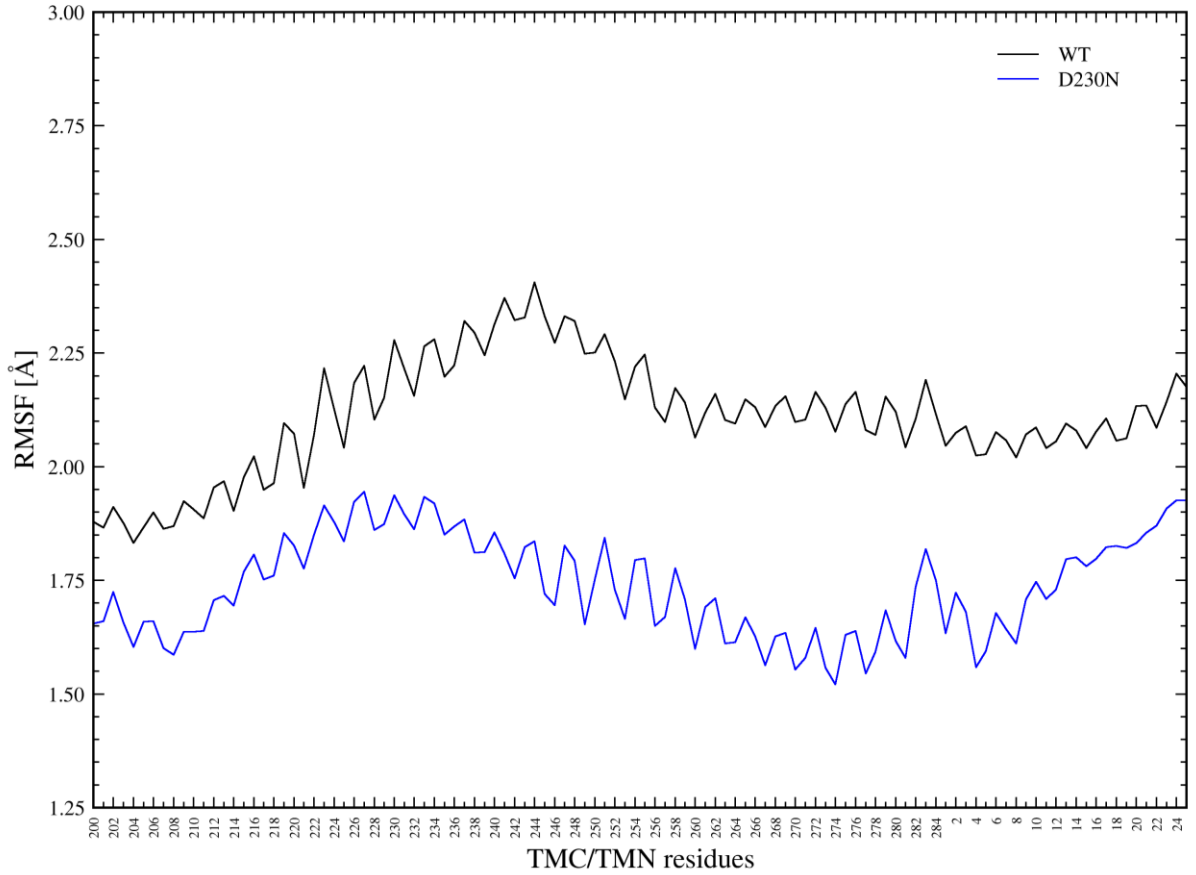
Mutational Effects on Thin Filament Stability and Interactions

To study the mutational effects on the stability and cooperativity of the regulatory thin filament, DSC was employed with fully reconstituted thin filaments (TF) composed of actin, TPM (WT-TPM, D230N-TPM, D84-TPM, or E62-TPM), and the wild-type troponin complex (cTnT, cTnI, and cTnC) (Figure 9 shows the location of TPM mutants within the TF all atom model). The first thermal transition within the plot corresponds to the C-terminus of TPM unfolding. The second domain represents the cooperativity peak of TPM and the Tn complex unfolding off of actin. The third and fourth domains represent the N-terminus of TPM unfolding and globular actin unfolding respectively. The D230N-TF showed the same stabilizing effect on both the TPM C- and N-termini as in the TPM dimer alone as seen by the rightward shift in the peak T_m values (D230N-TF, D1: 43.7 ± 0.02 °C, D3: 50.2 ± 0.06 °C; WT-TF, D1: 42.6 ± 0.05 °C, D3: 49.6 ± 0.09 °C) (Figure 10, Table 3). The cooperativity peak of D230N-TF (Domain 2) increased the unfolding temperature and narrowed the peak full-width-half-max (FWHM) value compared to WT (D230N-TF D2: T_m 46.6 ± 0.03 °C, FWHM 1.15 ± 0.03 °C; WT-TF D2: T_m 45.9 ± 0.08 °C, FWHM 1.65 ± 0.10 °C) (Figure 10, Table 3). The thermal shifts of the cooperativity peak are indicative of the strength of TPM-actin and TPM-TnT interactions, while the peak width is related to the adjacent TPM-TPM cooperativity with a peak narrowing suggesting a more cooperative system.

Figure 9: *Atomistic model (Schwartz et al.) of the cardiac thin filament and regulatory proteins. The thin filament is composed of actin (grey), TPM (green and orange) and the Tn complex, TnI is presented in blue, TnC in red, TnT is in yellow. The N-terminal of TPM in shown in orange and the C-terminal TPM in green. TPM mutant locations on TPM shown: D230N (red), D84N (green), and E62Q (cyan). Model image courtesy of Michael R. Williams, Schwartz group, University of Arizona.*
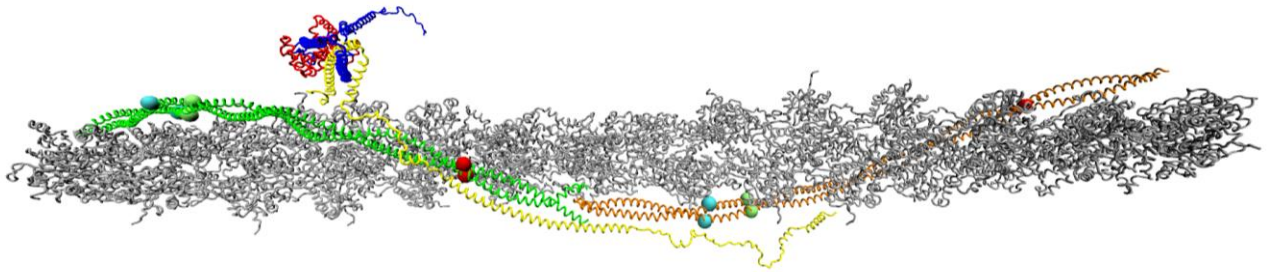
Table 3: Summary of DSC of the full thin filament data. All concentrations were between 1.3 and 2.0 mg/mL. The thermal unfolding temperature at the peak maximum is denoted by T_m (°C). The full width half max (FWHM) value is also reported. The values are reported as mean ± S.E.M. One-way ANOVA was used to determine statistical significance ****$p < 0.0001$, *** $p < 0.001$, ** $p < 0.01$, and * $p < 0.05$.

	DSC – Fully Reconstituted Thin Filament			
	Domain 1: TPM C-terminus	Domain 2: Cooperativity		Domain 3: TPM N-terminus
	T_m °C	T_m °C	FWHM (°C)	T_m °C
WT-TPM	42.6 ± 0.05	45.9 ± 0.08	1.65 ± 0.10	49.6 ± 0.09
D230N-TPM	43.7 ± 0.02***	46.6 ± 0.03*	1.15 ± 0.03*	50.2 ± 0.06*
D84N-TPM	39.7 ± 0.10****	43.1 ± 0.13****	3.09 ± 0.14****	50.4 ± 0.23*
E62Q-TPM	43.3 ± 0.04**	46.2 ± 0.19	2.40 ± 0.07**	51.6 ± 0.01***

Figure 10: *Differential Scanning Calorimetry of WT and D230N-TF reconstituted with Actin and a complete Troponin complex. Total protein concentration ~2 mg/mL in a ratio of 5:5:7 TPM:Tn:Actin (n=2,3 per group). DSC was scanned from 25-75 °C at a rate of 0.5 °C/min. These are representative images after subtraction of baseline and instrumental background. D1: TPM C-terminus unfolds, D2: TPM dimers unfold off actin, D3: TPM N-terminus unfolds, and D4: Actin unfolds.*
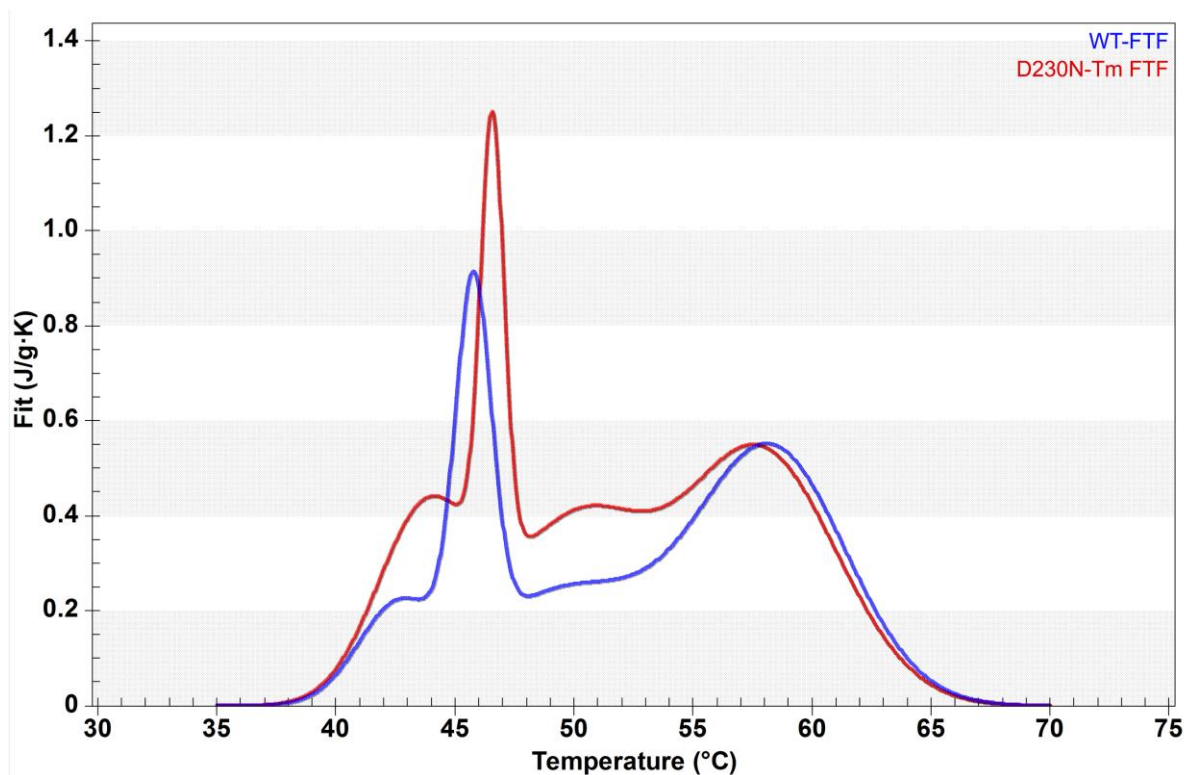
Consistent with DSC-TF data, molecular dynamic simulations run by the Schwartz laboratory compared effects of the D230N-TPM mutation within the full thin filament. In the presence of D230N-TPM, the flexibility and movement substantially decreases, represented by lower RMSF values at the residues near the TPM overlap (C-terminus 200-284, N-terminus 2-24) (Figure 8). The increases in rigidity within the D230N-TF is supportive of the TPM alone DSC and CD data (Figure 5 and 4 respectively). MD also revealed that D230N decreases the average distance between the TPM overlap region and cTnT (D230N-TF ~18.5 Å; WT-TF 21.0 Å), which is consistent with an increase in TPM-protein interactions of D230N-TF using DSC (T_m, D2) (Figure 11,12).

D84N-TF data for the TPM unfolding events paralleled the TPM-dimer alone data, destabilizing the C-terminus and stabilizing the N-terminus (D84N-TF, D1: 39.7 ± 0.10 °C, D3: 50.4 ± 0.23 °C; WT-TF, D1: 42.6 ± 0.05 °C, D3: 49.59 ± 0.09 °C) (Figure 13, Table 3), possibly decreasing communication between overlapping TPM dimers in the overlap region. D84N significantly increased the cooperativity peak width (FWHM), and decreased the thermal stability compared to WT (D84N-TF D2: T_m 43.1 ± 0.13 °C, FWHM 3.09 ± 0.14 °C; WT-TF D2: T_m 45.9 ± 0.08 °C, FWHM 1.65 ± 0.10 °C) (Figure 13, Table 3). These data suggest decreased interactions between D84N-TPM and surrounding proteins (decrease in T_m) as well as decreasing of the cooperativity of the system with significant peak broadening.

The HCM-causative and most N-terminal proximal mutation, E62Q, showed similarities to both DCM mutants individually. Both TPM termini showed a rightward shift in T_m (E62Q-TF, D1: 43.3 ± 0.04 °C, D3: 51.6 ± 0.01 °C; WT-TF, D1: 42.6 ± 0.05 °C, D3: 49.59 ± 0.09 °C), similar to D230N, although this is not consistent with the TPM alone data (Figure 14, Table 3). The cooperativity peak did not show a significant difference in T_m compared to WT-TF (E62Q-TF D2: T_m 46.2 ± 0.19 °C; WT-TF D2: T_m 45.9 ± 0.08 °C) (Figure 14, Table 3), although a substantial peak broadening occurred, (E62Q-TF D2: FWHM 2.40 ± 0.07 °C; WT-TF D2: FWHM 1.65 ± 0.10 °C) impacting the cooperativity (Figure 14, Table 3). The peak broadening would indicate decreased cooperativity for the TPM system, like D84N-TF.

Figure 11: Molecular Dynamics snapshots were taken from average structures from 3 production runs (each of 10 ns long). WT-TPM overlap region shown (green and orange), while WT-TPM effects (yellow), and D230N-TPM mutant effects (blue) on TnT position and protein separation. D230N structure was aligned to the WT structure by the backbone. This is a side view on both TnT and TPM, RMSD between WT and D230N for this section was 0.6527Å. Model courtesy of the Schwartz group, University of Arizona.
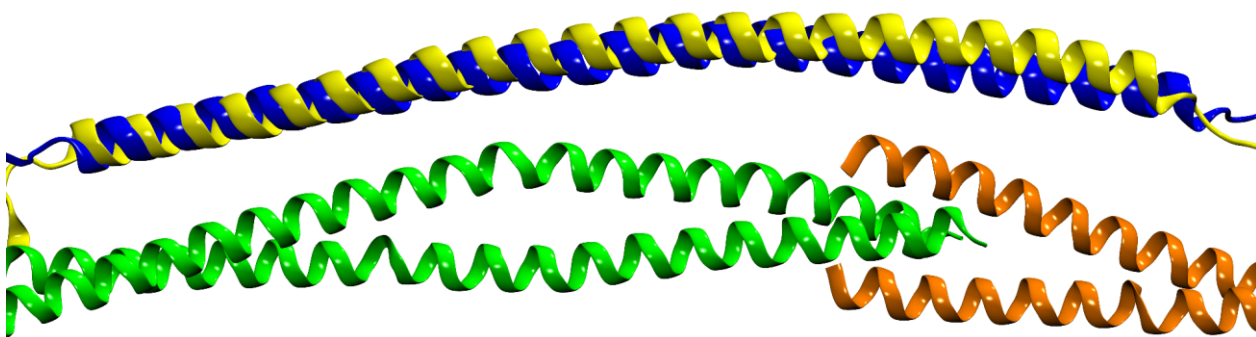
Figure 12: *Histograms were generated using a function for finding center of mass, implemented in VMD, then the distances between these points (in TnT and TPM) are measured for each snapshot in trajectory. The number of representatives in each bin was counted using a range of distances from 14 Å to 30 Å with steps 0.5 Å. Lukasz Szatkowski, Schwartz Laboratory, University of Arizona.*
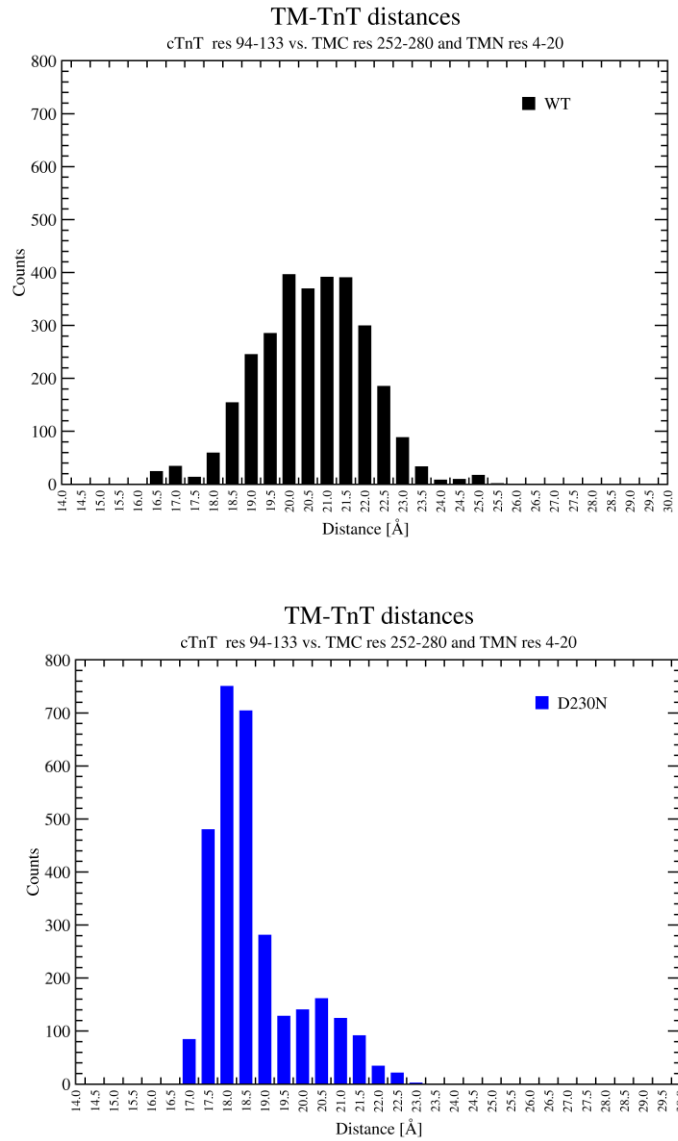
Figure 13: *Differential Scanning Calorimetry of WT and D84N-TF reconstituted with Actin and a complete Troponin complex. Total protein concentration ~2 mg/mL in a ratio of 5:5:7 TPM:Tn:Actin (n=2,3 per group). DSC was scanned from 25-75 °C at 0.5 °C/min. These are representative images after subtraction of baseline and instrumental background. D1: TPM C-terminus unfolds, D2: TPM dimers unfold off actin, D3: TPM N-terminus unfolds, and D4: Actin unfolds.*
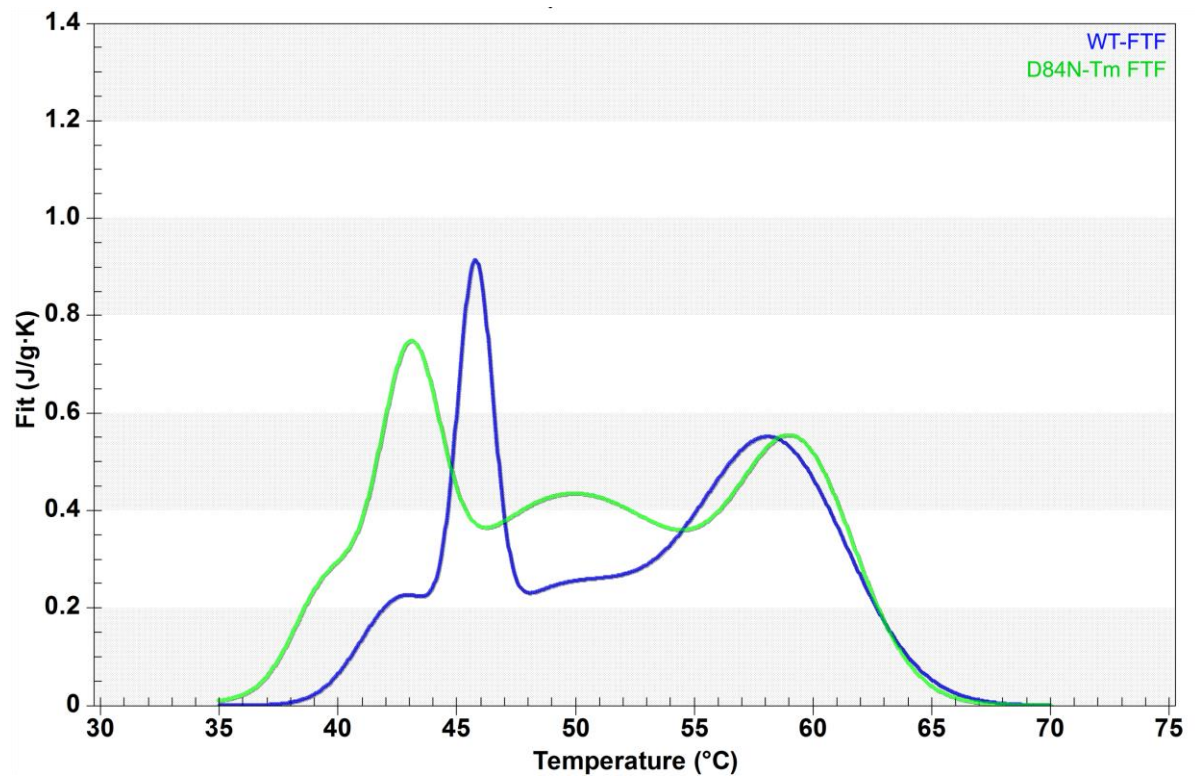
Figure 14: *Differential Scanning Calorimetry of WT and E62Q-TF reconstituted with Actin and a complete Troponin complex. Total protein concentration ~2 mg/mL in a ratio of 5:5:7 TPM:Tn:Actin (n=2,3 per group). DSC was scanned from 25-75 °C at a rate of 0.5 °C/min. These are representative images after subtraction of baseline and instrumental background. D1: TPM C-terminus unfolds, D2: TPM dimers unfold off actin, D3: TPM N-terminus unfolds, and D4: Actin unfolds.*
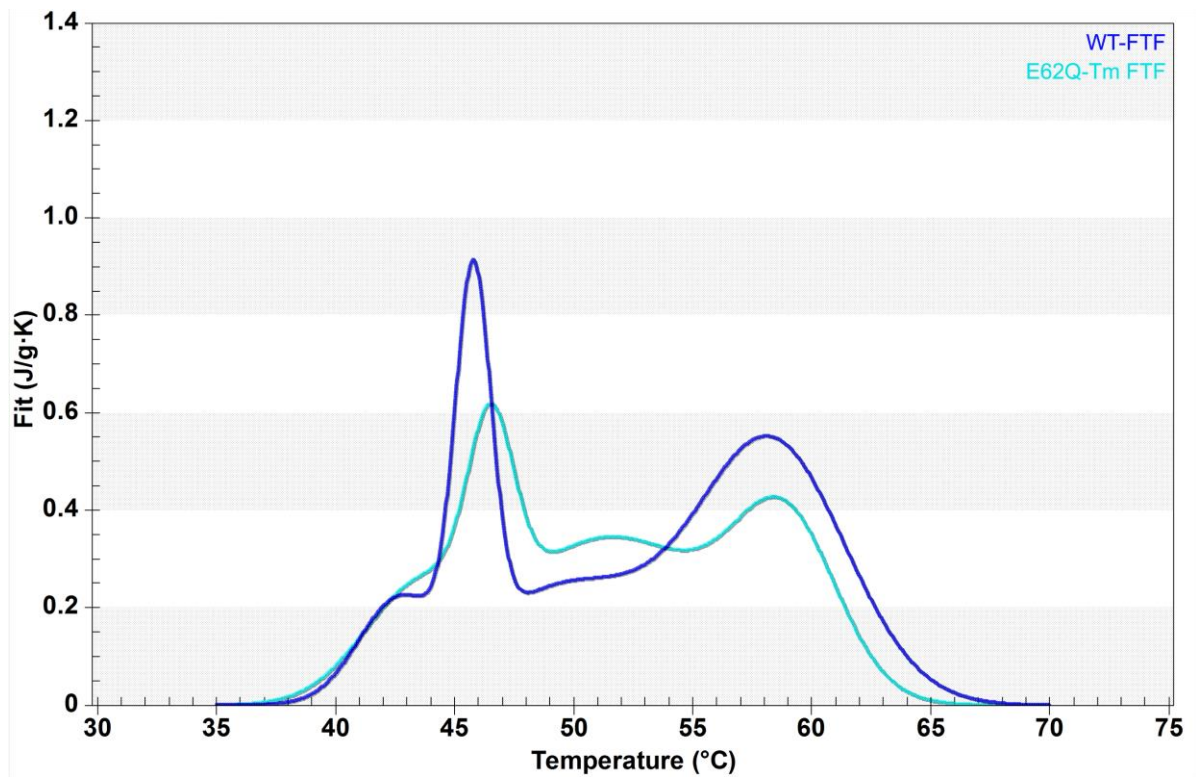
Actomyosin ATPase Activity and Ca^{2+} Sensitivity

The actomyosin cross bridge formation was measured by the ATPase activity of the system, with a faster ATPase activity related to the rate of cross bridge cycling. All mutants were normalized and compared to WT at $+Ca^{2+}$ (pCa =4.3) and $-Ca^{2+}$ (pCa=9). The D230N-TPM mutation showed a decrease in activation in the $-Ca^{2+}$ state and an increase in activity in the $+Ca^{2+}$ conditions (D230N-TPM $-Ca^{2+}$: 0.72, $+Ca^{2+}$: 2.72; WT-TPM $\pm Ca^{2+}$: 1.00) (Figure 15, Table 4). These data can be extrapolated to the TPM three-state-model equilibrium, with D230N-TF possibly indicating an increased barrier to activation, but once overcome, has increased activity. The D84N mutant showed a decrease in ATPase activity in both the deactivated ($-Ca^{2+}$) and activated ($+Ca^{2+}$) states (D84N-TPM $-Ca^{2+}$: 0.58, $+Ca^{2+}$: 0.71) (Table 4). This would imply an increased barrier to activation with and without calcium, biasing the equilibrium in the inactive state. Alternatively, the E62Q (HCM) mutant increased ATPase activity with and without calcium present (D230N-TPM $-Ca^{2+}$: 1.25, $+Ca^{2+}$: 1.10) (Table 4), consistent with a reduced barrier to activation as seen in other hypertrophic mutations in literature [21].

Calcium sensitivity was determined by the ratio of ATPase activity measured in the presence and absence of calcium ($\pm Ca^{2+}$). The calculated calcium sensitivity for WT-TF was 0.74 (Table 4). This value is comparable with the reported value of 0.78 [32] and indicates the formation of regulated

actin filaments. In comparison to WT-TF, the DCM mutants (D230N, D84N-TPM) decreased calcium sensitivity (0.20, 0.61 respectively), consistent with a known DCM compensatory response, while the hypertrophic E62Q mutant increased calcium sensitivity (0.84) (Figure 16, Table 4) [33].

Table 4: *Effect of TPM mutations on ATPase activity in the presence and absence of Ca2+ (pCa 4.3, pCa 9) and normalized to WT (n=1). Samples were reconstituted using rabbit skeletal myosin and actin, TPM and Tn with a final concentration of 1uM myosin, 4uM actin, 0.8uM Tn, and 0.7uM TPM in ATPase buffer. ATPase rate traces (with and without Ca2+) for TPM mutants were compared to WT, and independent mutational effects on Ca2+ sensitivity were determined (+ Ca^{2+} / - Ca^{2+}).*

Actomyosin ATPase Activity (± Ca^{2+}) and Calcium Sensitivity			
	Normalized ATPase Activity		Calcium Sensitivity (%)
	-Ca^{2+}	+Ca^{2+}	
WT-TPM	1.00	1.00	0.74
D230N-TPM	0.72	2.72	0.20
D84N-TPM	0.58	0.71	0.61
E62Q-TPM	1.25	1.10	0.84

***Figure 15:** Shows the ATPase activity traces of the TPM-mutations in the presence Ca²⁺ (pCa 4.3) (n=1). These representative traces were collected over 20 minutes and normalized relative to WT-TF to show the percent change. The steeper slope represents an increased rate. The slope measurements from 8-12 minutes were used for analysis.*
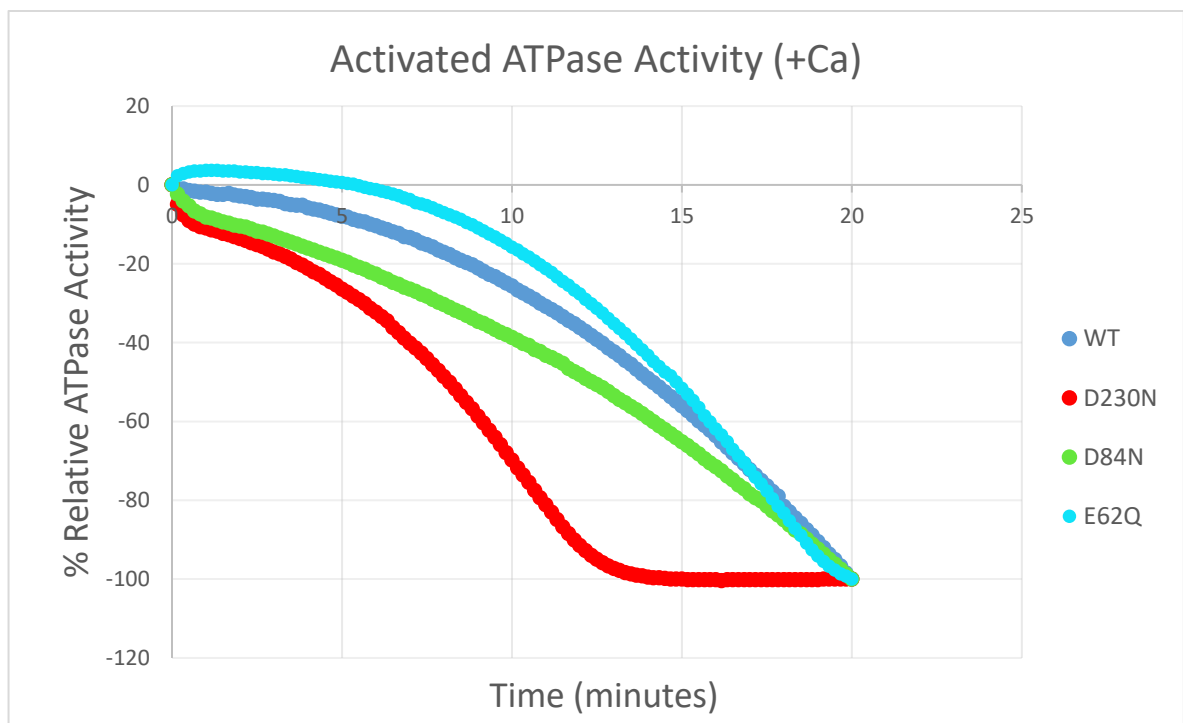
Figure 16: *mutational effects on Ca2+ sensitivity was determined based on the ATPase rates at ± Ca²⁺ (+ Ca²⁺ / - Ca²⁺). WT-TF value, 0.74, is consistent with literature to show that the filaments have properly formed. D230N-TF and D84N-TF indicate a decreased sensitivity, while E62Q-TF increases compared to WT.*
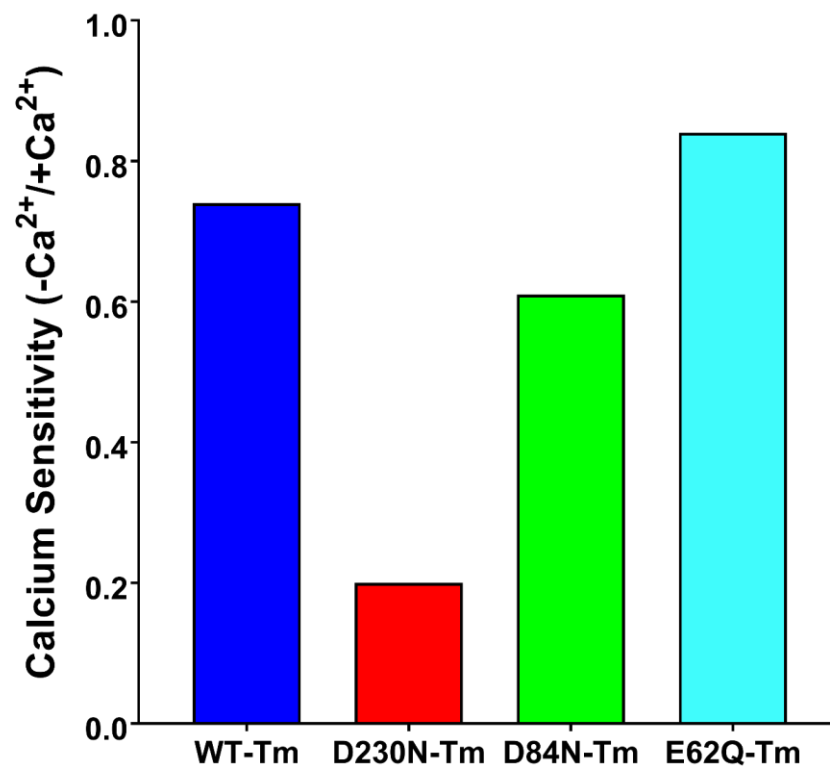
Discussion

Mutational Effects on Tropomyosin Structure

CD was used to access alterations in helicity and thermal stability of TPM secondary structure. D230N-TPM helical structure showed no significant change in the ellipticity compared to WT (Figure 4, Table 1), which was not surprising, as TPM is nearly 100% alpha helical, and significant changes in the helicity would impact viability [34]. The overall thermal stability of D230N-TPM, however, was significantly increased, resulting in a more rigid (less flexible) TPM. It should be noted that the use of the term "flexibility" to describe changes in the thermal stability of TPM has been well established in previous publications, and will be used for the entirety of this discussion [21,35,36].

Although CD did not reveal significant differences in the helicity between D230N-TPM and WT-TPM monomers, it revealed an increase in the thermal stability compared to WT. To collect more regional data on the mutant's structural effects, DSC was employed. This sensitive and reproducible technique has the power to inform on the thermal stability of both the C- and N- terminal regions of the molecule and determine the location and magnitude of the mutational impact on TPM structure. The thermal stability of D230N-TPM revealed an overall stabilizing effect of the mutation compared

to WT-TPM, indicating a less flexible dimeric structure. More specifically, there was an increase in T_m for both the C-and N-termini (Figure 5, Table 2). An increase in the unfolding temperature requires a greater energy input to denature the termini, suggesting stronger TPM monomer interactions at the ends and a more helical dimer structure.

These results are supported by MD simulations that demonstrate thin filaments containing D230N-TPM have lower average root mean square fluctuation (RMSF) values compared to WT at every TPM residue queried within the termini (Figure 8,12) [Schwartz Laboratory]. The RMSF represents the mobility of a residue's alpha-carbons during a trajectory. Smaller RMSF values at every TPM residue represent a decrease in flexibility or movement possibilities for D230N-TPM within the termini specifically. These results correlate with the in vitro studies in how the structural changes at the termini are affecting the cooperativity of the crucial TPM overlap region.

The other DCM-causing mutation, D84N showed destabilization of the C- terminus, while stabilizing the N-Terminus, corresponding to a left and right shift respectively (Figure 6, Table 2). This would correspond to a less helical C-terminus and a more helical N-terminus, possibly creating weaker interactions between TPM monomers at the ends. The D84N mutation showed the most pronounced left shift at the C-terminus (3°C), and a large (2°C) rightward shift at the N-terminus. While all other mutants studied lie on the

54

exterior, solvent exposed portion of the helix, D84N lies within the "g" position of the alpha-helical structure of TPM, and is known to form core stabilizing salt bridges in the 2nd period of TPM, a secondary actin binding site. Positively charged amino acids are in the corresponding "e" positions, supporting the formation of salt bridges and stabilization. When comparing the effects of both DCM-causing mutations, D84N-TPM would be expected to have a larger impact on the TPM structure due to disruption in the stabilization of the dimer core, whereas D230N-TPM could have a larger effect on interacting proteins within the TF that would not be evident in the TPM dimer alone [37].

E62Q-TPM causes a rightward shift at the N-terminus domain and left shift at the C-terminus domain, indicating weaker interactions between TPM monomers at the termini, like D84N-TPM, yet these two mutations result in different diseases and impairments. The E62Q mutant is the most N-term proximal mutation and had the largest effect on the N-terminus, increasing the unfolding temperature ~2.5°C (Figure 7, Table 2). E62Q mutant lies in a "secondary" actin binding site in the 2nd period of TPM [37]. Thus, the structural differences seen between the D230N, D84N, and E62Q suggests that the position on the alpha helix, location on TPM, and purpose could impact the mechanism in which these mutations lead to disease.

The DCM-causing mutations (D230N, D84N) increased the total enthalpy (ΔH_{cal}) to unfold the TPM-dimer, while the HCM-causing mutant

(E62Q) decreased the total enthalpy (Table 2). The enthalpy of the unfolding process is due to the breaking of hydrogen bonds and the denaturation of the alpha-helix, exposing the hydrophobic core region into water. At the peak of the transition, the Gibbs Free Energy is constant and can provide information about the entropy of the system via Gibbs free energy equation ($\Delta G = \Delta H - T\Delta S$) [31].

In the presence of D230N-TPM, both termini increase in thermal stability and enthalpy (Table 2). Holding Gibbs free energy constant, this would imply a decrease in entropy of the system, which is consistent with CD and MD data that suggested a more rigid, less disordered TPM dimer structure that could impair its function. Showing the opposite effect, the E62Q mutation increases the entropy overall, increasing the flexibility of this dimer. An increase in conformational disorder may allow the E62Q-TPM to bind to different sites on actin, potentially compensating for this substitution and shift as necessary to regulate myofilament activation. However, too much flexibility could potentially impair the cooperative movement of adjacent TPM dimers during regulation of contraction.

For all mutants, the more proximal termini required a greater percentage of the total energy (ΔH_{cal}) to unfold and decreased entropy. The D230N mutation is the most C-terminal proximal mutation, and has a largest increase (12%) in enthalpy required to unfold the C-terminal domain. This is

consistent with the increase in C-terminus thermal stability (T_m) of D230N, and indicates deficits at the overlap region due to a more helical structure (Figure 5, Table 2). DSC results on D84N and E62Q significantly increased the energy input required to unfold their proximal, N- terminus, by 21% and 26% respectively (Table 2). The increase in enthalpy corresponds with an increase in stability (decrease in entropy) of the N-termini (shown in DSC), and more stable, helical structure. The entropy of the C-terminus was increased, shown by a decrease in enthalpy for D84N and E62Q (21% and 26% respectively) indicating a less helical TPM dimer and less interactions at the overlap.

It has been proposed by Hitchcock-DeGregori that local disorder or instability is a general requirement for the regions of tropomyosin involved in binding to actin, or other target proteins [35,36]. It is necessary for adjacent TPM to form a continuous flexible cable along the length of actin for cooperative azimuthal movements in response to regulatory signals; an increase in the rigidity would be more difficult for adjacent TPM to shift cooperatively as a larger signal would be required to initiate movement [35].

It has been shown in proteins that bind a variety of targets, like calmodulin, that the flexibility of the recognition domains is critical for their ability to dynamically orient for optimal interactions. Our results indicate that the flexibility of the TPM dimer, paramount to the regulatory function of the thin filament, is compromised in the presence of the D230N, D84N, and E62Q

57

mutations, which could lead to the observed pathology. Furthermore, these data suggest an intrinsic link between the flexibility of TPM, phenotypic cardiac pathology, and regulatory function.

As these mutations are causative of disease it is not surprising that the effects propagate to the overlap region, and thus a system level. In fact, previous studies have demonstrated that a TPM variant (D137L) causes small local changes in flexibility that propagate much larger effects to a site 38 amino acids away [28,29] and more recently it was revealed that D137L alters the flexibility of TPM leading to changes in the regulatory function of the protein [21]. To further elucidate how each of these mutations (D230N, D84N, and E62Q) are leading to disease, it is necessary to increase the physiological complexity to examine the structural changes within the full thin filament.

Mutational Effects on Thin Filament Stability and Interactions

Regardless of location and proximity of the TPM mutation, structural alterations propagate to both termini, indicating that there could be an impact on the stability of the crucial overlap region, potentially altering the regulatory function of TPM (Figure 8). Despite its importance in modulating cooperative activation of the thin filament, the structure of the overlap is still not fully resolved. This is due to its dynamic nature, a property which creates difficulties when crystallizing the overlap. Another factor which makes the overlap difficult to study is its integration into a much larger thin filament complex of proteins. Thus, studying the TPM overlap in its native conformation on the thin filament is heavily constrained, since the whole thin filament cannot be studied at a high enough resolution via electron microscopy (EM) or X-ray crystallography [38,39]. DSC performed on the fully reconstituted thin filament was used to measure thermal stability and dissociation rate which is used to deduce changes in cooperativity between adjacent TPM at the overlap and TPM-protein interactions in the presence of a mutant. Although this is a steady state technique, the structural alterations will allow us to infer alterations in dynamic properties by which these mutations lead to disease.

The D230N-TPM mutation stabilized both the C- and N- TPM termini, represented by a rightward shift in domain 1 and 3 respectively, consistent with the TPM dimer alone structural changes. This indicates D230N-TPM

59

results in increased interactions at the termini and more helical structure. This would suggest more interactions in the TPM-TPM overlap region, potentially creating a tighter "lock." The cooperativity of the overlap region was correlated to the rate of the TPM and Tn dissociation from actin, represented by the sharpness (FWHM) of the transition peak. This hypothesis was confirmed with the D230N-TPM mutant causing a narrowing in the peak width (FWHM), indicating a less flexible, more cooperative TPM overlap region. These results are consistent with the MD (RMSF) and DSC dimer enthalpy results, demonstrating an increase in structural rigidity in the presence of the D230N mutation.

The thermal unfolding temperature of cooperativity peak represents the strength of TPM-actin and TPM-TnT interactions as the TPM dissociates from the thin filament. The D230N mutant is located on an exterior position on the alpha helix, solvent exposed and lies between two TPM-TnT binding regions at TPM-residues ~190 and 258 [37]. The D230N mutation propagates its effects to both ends of the TPM structure and could affect interactions and potentially the stability of the ternary complex between TPM, actin, and TnT. An increase in the T_m shows that the structural changes in D230N TPM are increasing the interaction strength with the other proteins within the TF (actin and Tn complex) (Figure 10). It has been shown using molecular dynamics that the structural changes occurring in the presence of the D230N-TPM mutation

60

cause the average distance between the overlap region of D230N-TPM and TnT to decrease (Figure 11, 12). The canonical coiled coil structure and flexibility at the C-terminus are critical features for TPM binding to TnT and it is imperative for the function of TPM that the N-terminus of TPM forms a binary overlap complex with the C-terminus of TPM in order to facilitate a ternary complex with the N-terminus of TnT [37]. Over-stabilization at this overlap region could explain the corresponding increase in interactions with TnT and functional impairment.

During cardiac contraction, adjacent TPM dimers transmit signals in succession to coordinate the azimuthal shift of TPM on actin, allowing myosin heads to weakly bind, pushing TPM out of the binding pocket. We believe that these results suggest that a more rigid TPM system with more interactions with TnT may be more difficult to move initially, as each TPM dimer is held firmly in place by the others, and would require a greater energy input (seen in DSC TPM dimer results) to counteract the increase in interaction strength. When this is overcome and movement is initiated, there would be enhanced response due to the increased rigidity, allowing myosin heads to bind strongly, quickly transitioning through the weak binding state.

The D84N-TPM mutation that is also DCM-causative shows opposite structural impacts on the full thin filament interactions and TPM cooperativity. The FWHM of the D84N cooperativity peak (domain 2) doubled

in comparison to WT-TF (Figure 13, Table 3). This would suggest a more flexible and less cooperative overlap region, where larger movements are required to generate the same response to adjacent TPM. This is again consistent with the interpretation of the TPM dimer alone data that implied a "looser" connection at overlap due to a less helical C-terminus and more helical N-terminus. The D84N mutant also has the largest impact on the TPM interactions with other proteins, decreasing the thermal stability by >2°C.

The decrease in D84N-TPM-actin interactions is consistent with published cosedimentation results that suggest a significantly diminished actin binding affinity caused by weakened charge-charge interactions. This is thought to be due to the disruption of an electrostatic salt bridge formation within the "g" position of the alpha helix, although D84N is also positioned in close proximity to positively charged residues on actin surface and may contribute to charge-charge interactions [3]. However, the destabilized and less cooperative TPM-TPM overlap region may also be impacting TPM-actin binding. It is imperative for the function of TPM that the N- and C-termini of TPM form a binary overlap to facilitate the ternary complex with troponin T. The formation of these complexes is required for TPM to bind to actin with high affinity, and to cooperatively regulate force generation [15,16]. The weaker connection created by the ends of D84N-TPM would not be able to properly form the ternary complex, destabilizing TPM-actin interactions as well. D84N

and D230N DCM mutants have shown opposite structural effects on the thin filament, suggesting that the location on TPM and within the alpha helical wheel are important factors that influence the mechanism by which each mutation uniquely leads to disease.

E62Q effects on the TPM alone have many similarities with the D84N DCM-causing mutation, although the E62Q mutant lies within the 2nd period of TPM in an externally exposed f-positon, within an actin binding site. Glutamic acid 62 is thought to be a strategically placed acidic residue on the TPM-surface that can electrostatically interact with positively charged residues present on the complementary flat face of actin subunits within thin filaments [37]. Actin binding sites are distinctive in their contributions to the overall affinity, as well as to the cooperativity of binding [40]. These electrostatic interactions are weak, but stereo-chemically specific and can be easily perturbed by the substitution of a polar, uncharged glutamine.

E62Q-TF showed a significant peak broadening of the cooperativity peak, like D84N-TF, indicative of a less cooperative TPM network. This is consistent with the DSC TPM dimer data, that there were less interactions and a weaker connection between adjacent TPM dimers and decrease in total enthalpy. Although, the E62Q-TPM thermal stability of these domains in the full thin filament were not consistent with TPM alone data. E62Q-TF TPM domains 1 and 3, corresponding to the C- and N- termini respectively, show

stabilization of the structure with a rightward shift, in comparison to E62Q-TPM dimer destabilizing the C-terminus with a leftward shift (Figure 7,14). As both results are highly reproducible, we hypothesize that this increase in stability of the C-terminus could be due to a stabilizing mechanism in the full thin filament.

The TPM C-terminus and overlap region within the full thin filament is stabilized by the N-terminus of troponin T and interactions with actin, forming the ternary complex [15]. In the presence of the E62Q mutation, this is consistent with the slight rightward shift in the unfolding temperature of the cooperativity peak, corresponding to increased TPM-protein electrostatic interactions to potentially stabilize the overlap region. However, this shift was not a statistically significant change in the thermal stability (T_m), which is surprising considering the E62Q mutation lies within an actin binding site but could be explained by an increase in conformational disorder (seen by DSC-TPM dimer data). The increase in flexibility (disorder) of the E62Q-TPM may provide it with more ability to bind actin, potentially compensating for this substitution and shift as necessary to regulate myofilament activation.

The E62Q-TF cooperativity peak thermal stability measurements have a significantly higher SEM than most DSC data, which would lend support to the hypothesis for this potential compensatory mechanism. The fluctuations in T_m for this peak may also be explained by the fact that all TPM-TF protein

64

interactions are measured simultaneously, without enough resolution to segregate the contribution from specific TPM-actin interactions. In addition, the E62Q mutation lies within a secondary actin binding site in period 2. The primary actin binding sites (P1, P5) contribute more to the overall actin affinity than secondary sites (E62). It is suggested that the secondary sites may bind to and modulate interaction with actin following initial binding via one of the primary sites, which would also be consistent with these findings, as the full thin filament should be primarily modulated by primary actin binding and E62Q should have a smaller effect [5].

Together, these data suggest that the mechanisms leading to disease are unique for each mutation. The precise link(s) between impaired activation and complex cardiac remodeling require further study in a dynamic system.

Actomyosin ATPase Activity and Ca²⁺ Sensitivity

The D230N mutation induced structural changes implied alterations in TPM flexibility, TPM-TPM cooperativity, and interactions that could impair the regulatory function of TPM. To characterize the resultant functional deficits of these structural perturbations, actomyosin ATPase activity in the presence and absence of calcium was performed to monitor changes in actomyosin activation.

D230N-TF showed a decrease in ATPase activity in the absence of calcium, and an increase in actomyosin activation in the presence of calcium. Overall, the D230N-TPM mutation decreases in calcium handling are typical of DCM-mutations [33]. These functional deficits may demonstrate an equilibrium bias between the blocked, closed, and open states of TPM. In combination with the structural effects on flexibility and the overlap region, we are able to generate hypotheses about the mechanism causing the bias.

At low Ca^{2+} levels, the rigidity of the D230N-TPM (CD and DSC-TPM) and increased interactions could prevent its movement resulting in the observed decrease in Ca^{2+} sensitivity (Figure 16, Table 4). However, when excess Ca^{2+} is present in the activated state, the transition from the closed (C) to open (O) state occurs more rapidly. Once the myosin heads bind weakly to actin in the closed state, they are able to push the rigid and highly cooperative TPM out of the groove, propagating this activation to the neighboring

filaments, thus, increasing the rate of ATPase activity (Figure 15, Table 4). Together, these changes could indicate a biased activation equilibrium, in which the closed position becomes an activation barrier (Figure 17).

Although both D230N- and D84N-TPM are DCM-causative, the D84N mutation demonstrated a different functional impact. The D84N-TPM caused a more rigid structure and less cooperative TPM-TPM overlap region, biasing the three-state equilibrium differently. The decrease in the ATPase activity in the inactive state and active state, and decreased calcium sensitivity suggests that at any given Ca^{2+} concentration it is more difficult to initiate the same response to activation as WT. It is more difficult to transition from the blocked (B) to closed (C) state, via the increased rigidity, as seen by an overall increase in enthalpy in the TPM-dimer alone, especially at the N-terminus proximal to the mutation (Figure 17). Even as Ca^{2+} levels rise, the decrease in cooperativity between adjacent D84N-TPM would prevent the propagation of movement to neighboring filaments, leading to an activation barrier and further biasing the equilibrium from the open to closed state.

Both DCM-mutations demonstrated a decrease in calcium sensitivity while HCM-causative E62Q showed an increase in calcium sensitivity compared to WT, consistent with literature [33]. E52K-TPM and E40K-TPM (DCM mutations) are also associated with a decreased Ca^{2+} sensitivity possibly as a consequence of a weakened calcium-on interaction [3]. To compensate for

this decrease in sensitivity, transient Ca^{2+} amplitudes increase to generate the same response as WT myofilaments [41]. Of note, given the above described differences in primary structure, the conclusions drawn from the steady-state Ca2+ sensitivity assay are likely not representative of this highly dynamic, complex system. We believe that the decrease in calcium sensitivity is a result of unique structural perturbations that cause different functional deficits, modeled by the bias in the three-state-model.

Functionally, the E62Q mutant showed the typical "hypercontractile" profile, demonstrating an increased calcium sensitivity, and ATPase activity [4]. In the presence and absence of calcium, the rate of ATPase activity was elevated, potentially indicating a faster transition from the blocked to open state with little time spent in the closed state due to the increased sensitivity and activation with calcium (Figure 17). This fast transition from the blocked to closed states could be due to the increase in entropy, and thus, flexibility of the E62Q-TPM dimer. While this faster transition does not follow what would be expected with a decrease in TPM cooperativity seen via DSC, these results could potentially be explained by an increase in thermal stability, and increased interactions, potentially stabilizing the C-terminus with the ternary complex. Further investigation is required to fully establish these trends.

To support these conclusions, it was recently shown that HCM-linked mutations in the Tn-binding site of TPM (I172T, L185R, and E180V) all cause

differential effects on the thermal stability of TPM, despite being phenotypically similar [42]. This study and the results presented in this thesis further demonstrate our incomplete understanding of how single amino acid mutations lead to a complex series of cardiomyopathies and underscore our need for accurate models and targeted therapies. It is likely that mutations in the regulatory TPM that alter its thermal stability and flexibility lead to disease in a specific manner dependent on the precise amino acid change and location (periodically and helically) on TPM. This data, in combination with additional *in-vitro* and *in-vivo* testing will be used in the development of a technique "toolbox" to determine the mechanisms by which these TPM mutants lead to disease. This study highlights the complexity of interpretation of results from this system and thus will require multiple layers of resolution to determine how these mutations lead to disease.

Figure 17: *TPM three-state-model bias for D230N-TPM, D84N-TPM, and E62Q-TPM mutants. These results were hypothesized based on results from DSC-TF, ATPase activity (± Ca²⁺), and calcium sensitivity. The atomistic model of the thin filament from Manning et. al, Biophys J. Aug 30; 50(34): 7405-7413.*
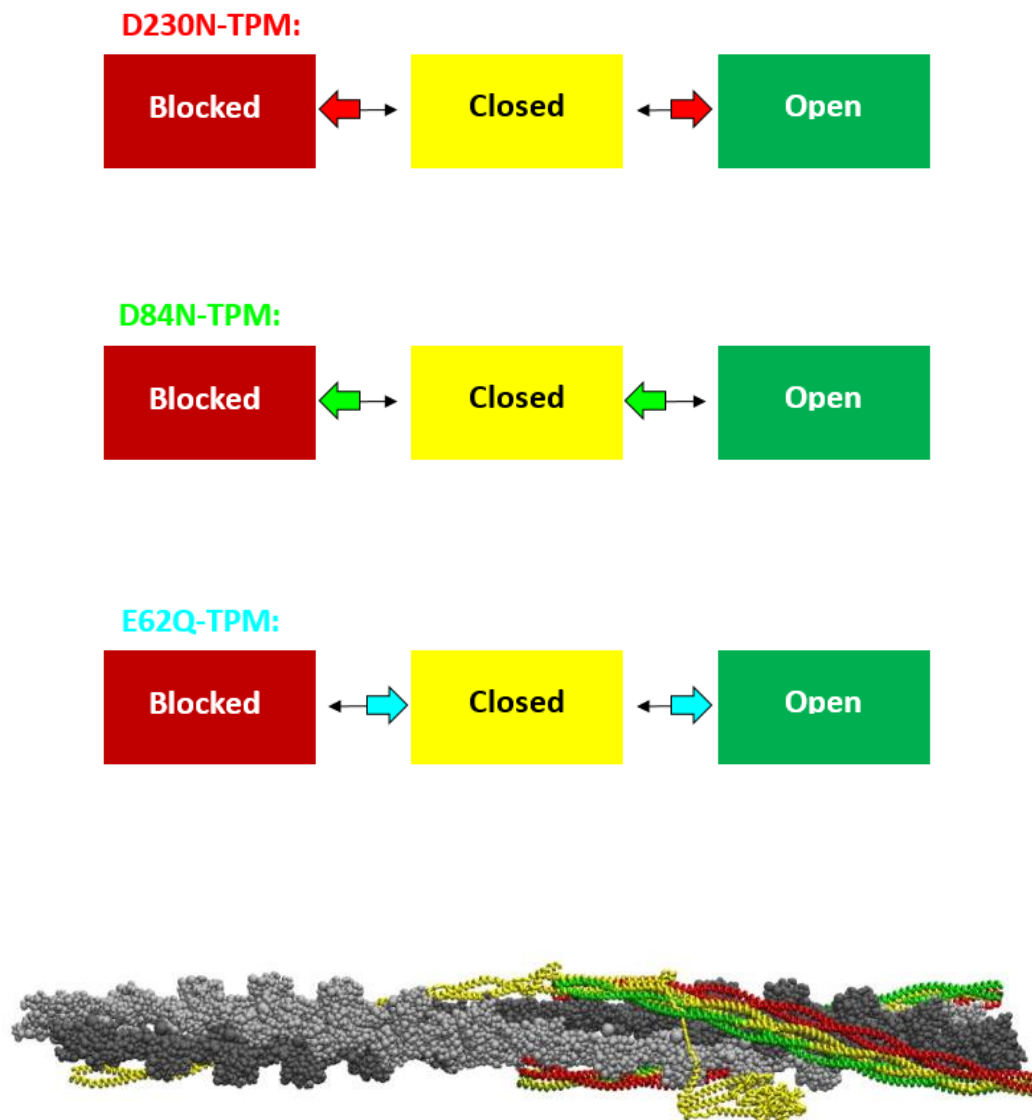
Conclusions and Future Directions

Overall, these data have shown that the structural effects of a single amino acid point mutation can propagate to the critical TPM-TPM overlap region and effect the regulatory properties of the thin filament. Currently, there are over 100 sarcomeric mutations that are known to be causative of HCM or DCM and many more are implicated in disease [29]. These data show that the mechanisms leading to disease are unique and the current paradigm of the field to mechanistically classify HCM or DCM based on their phenotype may be inaccurate [4].

In this thesis, I have presented a multi-modality approach, to establish the link between biophysical insults of mutations and the remodeling and disease that occur in patients. The primary biophysical effects of these mutations were studied *in-vitro* via circular dichroism (CD), differential scanning calorimetry (DSC), myofilament activation, and calcium sensitivity (ATPase assay). This work was presented in conjunction with *in-silico* studies from our collaborators in the same region.

The D230N mutation, causative of a dilated cardiomyopathy, progresses to disease through an increase in stability and rigidity of TPM leading to a more cooperative overlap region in the thin filament (Table 5). There was an increase in protein-protein interactions, which corresponds with a decrease in

distance between TPM and TnT in the presence of D230N-TPM. Functionally, D230N shows a decrease in calcium sensitivity and bias three-state model of myofilament activation. The D84N-TPM mutation, also DCM-causative showed an increase in overall rigidity of TPM, but created a weaker connection in the overlap region and a less cooperative TPM network. D84N destabilized protein interactions and functionally impaired the regulatory properties of TPM, shifting the myofilament activation away toward inactivation.

The E62Q, HCM mutation, showed structural similarities to both DCM mutants, with a looser connection at the overlap and decreased cooperativity between adjacent TPM dimers. E62Q-TF did not show a statistically significant change in protein interactions compared to wild-type, which was surprising because it lies within an actin binding pocket. The E62Q mutation showed a unique combination of stability and flexibility of the structure of the E62Q-TPM dimer alone vs. E62Q-TF that suggests the potential for an underlying stabilization of the C-terminus through interactions with actin and formation of the ternary complex. Increased actomyosin activation of E62Q agreed with commonly associated properties of HCM mutations, biasing the three-state-equilibrium to a more activated state and increasing calcium sensitivity. These data have shown that the structural effects of a single amino acid point mutation can propagate to the critical TPM-TPM overlap region and

Table 5: *Summary of results to elucidate potential mechanistic patterns of DCM-causing D230N, D84N-TPM mutants and HCM-causing E62Q-TPM.*

			Structural and Functional Patterns for TPM Mutants							
	Literature Values					DSC TF: Cooperativity Peak		ATPase Assay		
	Protein	Phenotype	Actin-binding	Tm Helical position	Tn-binding	T_m °C	FWHM	$+Ca^{2+}$	$-Ca^{2+}$	Calcium Sensitivity
D230N -TPM	Tm	DCM	X	f	√	↑	↓	↓	↑	↓
D84N- TPM	Tm	DCM	√	g	X	↓	↑	↓	↓	↓
E62Q- TPM	Tm	HCM	√	f	X	N/C	↑	↑	↑	↑

affect the regulatory properties of TPM, biasing the three-state-model equilibrium (Figure 17).

Although the complete mechanisms of disease were not elucidated with this data alone, it provided us with valuable information about the system and primary disease progression. However, these techniques are not representative of cardiac physiology without physiological load that would be present in the heart. Lauren Tal Grinspan a previous graduate student in the Tardiff Laboratory generated a transgenic D230N-TPM mouse model that phenocopies the human disease. I am currently in the process of developing a mouse model for the D84N-TPM mutation for the comparison of these two DCM-causing mutations *in-vivo*. Additionally, these mice will measure *in-vitro* force pCa curves on a loaded fiber system, which would provide a better representation of the mechanistic and physiological differences that are known to exist in the human population.

Additionally, we claim that different levels of resolution and complexity are required to elucidate a mechanism due to the complexity of the system. Many hypotheses have been developed from this data (Figure 17), but it is clear that further *in-silico, in-vitro* and *in-vivo* testing will be required to determine the complete mechanisms leading to pathological remodeling. Our collaborators at the Schwartz laboratory are currently developing models for the D84N and E62Q-TPM mutations to support DSC structural data that will

74

allow us to predict structural changes and interactions between proteins. In the future, we hope that these computational methods can become a screening technique that will allow us to predict thin filament mutational effects that can be validated via numerous *in-vitro* techniques. The ultimate goal of this project is to create a "toolbox" of techniques that would provide data with mechanistic patterns with the ability to predict an unknown phenotype given a known genotype. This would also allow for improved mutation-specific therapeutic interventions to ultimately prevent disease progression in patients.

Methods

Site directed mutagenesis:

alanine-serine alpha tropomyosin (as-TPM) had been previously inserted into the pET3D vector (Novagen) by Lauren Tal Grinspan. as-TPM is used to mimic acetylated N-terminus of TPM that is found *in-vivo,* which is necessary for proper binding of TPM to actin, as well as proper head to tail formation of the overlap [41]. Mutations were incorporated into the plasmid via the Quikchange XL II site directed mutagenesis kit (Qiagen). Specific primers were designed to incorporate the mutation in the plasmid via the Quikchange primer design program (Qiagen). These primers are designed to handle the thermodynamic instability associated with mismatched nucleotides compared to the parental strand. PCR is then performed using a high-fidelity DNA polymerase, the parental DNA, the designed primers, dNTPs, and an optimized buffer. Dpn1 is then used to digest the parental DNA from the *E.coli*, as they are methylated, and thus targeted by Dpn1 digestion. 2 uL from the pre-digested sample and 2 uL post-dpn1 were run on an agarose DNA gel to confirm complete digestion.

The isolated mutant DNA is then transformed into XL-10 gold cells which repair the mutant plasmid DNA, which if unrepaired, would result in inefficient protein expression. The XL-10 gold cells are then transformed onto

LB-agar + Ampicillin plates to select for bacteria which contain the mutant plasmid that carries the Ampicillin resistance gene. XL-10 gold cells are endonuclease deficient, which improves the quality of the resultant miniprep DNA [43]. Once the colonies are formed, at least 3 colonies are grown in 5 mL of LB + ampicillin broth each to prepare DNA for isolation.

DNA is harvested via the use of a Plasmid DNA mini-prep kit (Qiagen). The bacteria are first pelleted from the media. The pellet is re-suspended in 250 uL of resuspension buffer. 250 uL of lysis buffer is added and the pellet reacts for 5 minutes. 350 uL of neutralization buffer is added, creating a cloudy lysate. The lysate is removed via centrifugation, while the supernatant is centrifuged over a column which binds to the DNA. The DNA is washed with an ethanol solution, and eluted using ddH_2O. The concentration of the resultant DNA is measured via a NanoDrop One (Thermoscientific). The plasmids are sequenced at the University of Arizona Genomics Core. The D230N-TPM plasmid was created by Lauren Tal Grinspan, a previous graduate student in the laboratory.

Transformation of cTnT,cTnC,cTnI, and as-TPM:

Minimal volume of BL21 ultra competent *E.coli* bacteria (25 uL) and the plasmids were thawed on ice from -80 °C, and -20°C respectively. When the BL21 bacteria thawed, 1 uL of plasmid DNA was added to the tube, gently

shaken via tapping, and allowed to rest on ice for 20 minutes. The BL21 + DNA mixture was then heat-shocked at 42 °C for 45 seconds, and then allowed to rest on ice for 2 minutes. A volume of SOC media equal to the BL21 + DNA mixture was added to the tube, which was then allowed to shake at 250 RPM at 37 °C for 30 minutes. Finally, the bacteria was plated onto LB Agar + Ampicillin plates to allow for growth of only the bacteria which incorporated the pET3D vector.

cTnT was expressed via Rosetta cells instead of BL21 due to the presence of rare codons, otherwise, the remainder of the transformation protocol is identical. The transformation and purification of all components of the troponin complex were performed by Dr. Mark T. McConnell, a previous graduate student in the Tardiff Lab.

Growth of bacterial cultures:

Colonies of bacteria were selected for inoculation based upon being visibly isolated from other colonies to avoid inoculating non-ampicillin selected bacteria. The colony was transferred to 5 mL of LB + Amplicillin media and allowed to shake at 250 RPM, 37 °C for at least 5 hours or until turbid. 1 mL of bacteria as well as 1 mL of 1000x ampicillin and 1 mL of $MgSO_4$ was inoculated into 1L of media previously prepared: 2 L of ZYP media (20 g tryptone, 10g yeast extract, 10g glycerol, 4g lactose, 1g glucose) with 50 mL of

78

phosphate buffer added as an auto-induction media. Each 1 L of the media was autoclaved into a 4 L flask prior to use. The media was shaken at 250 rpm at 37 °C for 16-18 hours. The bacteria was pelleted using the Beckman-Colter JA-10 rotor at 4000 rpm for 15 minutes at 4 °C. Pellets were either stored at -80 °C for temporary storage or purified via protein-specific procedures.

Tropomyosin purification:

The pelleted proteins were re-suspended in 60mL of ddH_2O and lysozyme was added to the solution (1mg of lysozyme per 10mL of solution). The solution rested at room temperature for 60 minutes before 3 sonication cycles on ice (3minutes on continuous power 10, followed by a 3 minutes rest). The sonicated solution was then centrifuged using the JA-17 rotor at 14,000 RPM for 45 minutes. The resultant supernatant was then placed into a 50mL falcon tube which was placed into boiling water for 10 minutes, leading to denaturation of most of the proteins except TPM, which is very thermostable. The denatured proteins were then removed via centrifugation using the JA-17 rotor at 17,000 RPM for 15 minutes. The TPM was purified from remaining protein contaminants and DNA using acid and base cuts:

The supernatant resulting from the previous centrifugation was placed into a beaker, and 1 M HCl was added dropwise to the mixture. The drops would form white precipitates in the solution which dissolved before adding

additional drops. The pH of the solution was allowed to fall between 4.4-4.6. At this stage, the solution appeared opaque and yellow in color. The mixture was centrifuged using the JA-17 rotor at 17,000 RPM for 10 minutes. The tropomyosin pellet was then resuspended in 20 ml of 1 M KCl, and the pellets dissolved after adding of 1M KOH to the mixture until the pH adjusted to between 7-8. The solution was allowed to stir until most of the particles dissolved. Next, the solution was centrifuged using the JA-17 rotor at 17,000 RPM for 10 minutes. The acid and base cuts were then repeated at least 2 more times, until the 260/280 (DNA:Protein) ratio of the protein is acceptable (0.8 or below). The purity of the protein was verified via SDS-PAGE.

cTnC purification:

The bacterial pellets containing recombinant cTnC protein were resuspended in 40-80 mL of Q-Sepharose (6 M Urea, 50 mM Tris base, 1 mM EDTA, 0.3 mM DTT, pH 7.8). The suspended bacterial pellet was sonicated and then centrifuged for 30 minutes at 17,000 rpm in the JA-17 rotor (Beckman Coulter). The resultant supernatant and pellet were then sampled and run via SDS-PAGE to verify that the recombinant protein has been expressed in sufficient quantity. Once the protein was verified to be in the supernatant, it was loaded into a BioRad EconoColumn (BioRad, Hercules, CA, USA) which had been already cleaned and equilibrated with 1.2 L of Q-sepharose. After the

protein is fully loaded, the column was then re-equilibrated with at least 1.2L of Q-Sepharose. Next, a gradient elution from 0.0 to 0.6 M NaCl was performed on the column. Resultant fractions were examined via SDS-PAGE, and fractions containing cTnC were pooled, and dialyzed against 2 x 4 L of Phenyl-Sepharose buffer A (50 mM Tris HCl, 1mM $CaCl_2$, 1 mM $MgCl_2$, 50 mM NaCl, 1 mM DTT, pH 7.5). The cTnC was then loaded onto a column which had been cleaned and equilibrated. After loading the dialyzed protein, the column was re-equilibrated with 1.2 L of Phenyl Sepharose A. The protein was then eluted by running through Phenyl Sepharose C solution (50 mM Tris-HCl, 1 mM EDTA, 500 mM $(NH_4)_2SO_4$,1 mM DTT, pH 7.5). The resultant fractions were analyzed via SDS-PAGE. Fractions containing purified cTnC were kept. This preparation was performed by Dr. Mark T. McConnell.

cTnT Purification:

The bacterial pellets containing recombinant cTnT protein were resuspended in 40-80 mL of S-Sepharose (6 M Urea, 50 mM Tris base, 2 mM EDTA, 1 mM DTT, pH 7.0). The suspended bacterial pellet was sonicated and then centrifuged for 30 minutes at 17,000 rpm in the JA-17 rotor. The resultant supernatant and pellet were then sampled and examined via SDS-PAGE to verify that the recombinant protein has been expressed in sufficient quantity. Once the protein was verified to be in the supernatant, it was loaded into a

BioRad EconoColumn (BioRad, Hercules, CA, USA) which had been already cleaned and equilibrated with 1.2 L of S-sepharose. After the protein is fully loaded, the column is then re-equilibrated with at least 1.2 L of S-Sepharose. Next, a gradient elution from 0.0 to 0.6 M KCl was performed on the column. Resultant fractions were examined via SDS-PAGE, and fractions containing cTnT were pooled, and dialyzed against 4 L of Q-Sepharose Buffer. The cTnT was then pumped into the Q-sepharose column and purified via the same procedures as the cTnC protein including washing, equilibrating, re-equilibrating, eluting the column and verifying purity via SDS-PAGE. The fractions containing cTnT were pooled and stored for later use at -80 °C. This preparation was performed by Dr. Mark T. McConnell.

cTnI Purification:

Bacterial pellets containing cTnI were resuspended in s-sepharose buffer and then purified following the protocols that were performed for cTnT. This includes sonication, SDS-PAGE, cleaning and equilibration, running the protein in, re-equilibration, and elution. The eluted fractions were analyzed via SDS-PAGE, and the fractions containing cTnI were dialyzed against 4 L of TnC affinity buffer (50 mM Tris, 2 mM CaCl, 0.5 M NaCl, 1 mM DTT, pH 7.5). The cTnI was pumped into a regenerated and equilibrated column, and then re-equilibrated with at least 300 mL of cTnC Affinity buffer. An elution gradient

is then run with cTnC elution buffer. To make the elution buffer, 3 mM EDTA and 6 M Urea were added to the cTnC affinity buffer. After eluting the protein, fractions were analyzed via SDS-PAGE, and fractions containing protein were aliquoted and stored in -80 °C. This preparation was performed by Dr. Mark T. McConnell.

Acetone powder preparation:

Rabbits were sacrificed in accordance with NIH guidelines and approved by the Institutional Animal Care and Use Committee (IACUC) at the University of Arizona. Skeletal muscles from the rabbit were harvested, ground, and stored at -80 °C. 333g grams of actin were extracted using 1 L of Guba-Straub solution (300 mM KCl, 100 mM KH_2PO_4, 50 mM K2HPO4, pH 6.5). The solution was allowed to extract for 20 minutes. Next, the solution was centrifuged using the JA-10 rotor at 6000 rpm for 10 minutes. The pellets were then re-suspended in 1665 mL of 0.4% $NaHCO_3$ and 0.1 mM Ca solution. This admixture was allowed to stir for 30 minutes. The mixture was then filtered using a vacuum setup through three layers of cheese cloth. The residue that was trapped by the cheesecloth was then divided into two equal portions. Each portion was then mixed with 3330 mL of room temperature ddH2O. After mixing, the solution was then squeezed through two clean layers of cheesecloth. These residues are recombined and then 666 ml of cold (pre-chilled

83

4°C) acetone is added to the combined residue. The acetone-powder mixture was allowed to stir for 30 minutes at room temperature and then filtered through 3 layers of cheesecloth with suction, but no squeezing of the cheese cloth. The acetone treatment and filtering was repeated four additional times. The resultant powder was spread out on cheesecloth which is placed on aluminum foil on a bench top, in order to capture all of the acetone powder. The powder was allowed to dry out overnight. Once dry, the powder can be stored at -80 °C. Prior to actin extraction, the acetone powder should be blended by using a coffee grinder.

Actin extraction from Acetone powder:

4 g of acetone powder were extracted on ice with 80 mL of Buffer A with gentle stirring (10 mM Tris, 0.2 mM $CaCl_2$, 0.2 mM ATP, 0.2 mM DTT, pH 8.0). The solution was then vacuum filtered, and the filtered solution is placed onto ice. The resultant residue on the filter paper was then removed from the funnel, and re-extracted using 20 mL of Buffer A. This re-extracted solution is then filtered, and the resultant filtrate from the two extractions was combined, then spun at 17,000 rpm in the JA-17 rotor for 30 minutes. The supernatant from the centrifugations was then polymerized in a beaker at room temperature for an hour by adding 0.05 M KCl to the solution and 2 mM of $MgCl_2$ and gently stirring. This was performed by adding 1.7 ml of KCl and

196 uL of $MgCl_2$ per 100 mL of actin. The beaker containing the actin solution was transferred to 4°C and 4.2 g of solid KCl was added per 100 mL of actin solution. The solution was then allowed to stir for 1.5 hours. Next, the solution was centrifuged for at least 8 hours at 17,000 rpm using the JA-17 rotor. The supernatant was discarded, and the pellets were rinsed with Buffer A before letting the pellets soak in 0.5 mL of Buffer A overnight. The pellets are dissolved using a glass stirring rod, and homogenized for about five minutes until the solution was clear. The resultant F-actin was dialyzed against Buffer A for three days, while mixing the bag every few hours and changing the dialysis buffer every day. As a result of the dialyses, the F-actin should have depolymerized to G-actin. The G-actin was then centrifuged at 17,000 rpm in the JA-17 rotor for 45 minutes. The supernatant was kept, and the concentration was determined via absorbance spectroscopy measuring at 290nm, $\varepsilon= 26,600$ $M^{-1}cm^{-1}$. The G-actin can be stored on ice with 0.1 mM NaN_3. Prior to use in the thin filament, the actin can be polymerized by slowly stirring while adding 1.7 ml of KCl and 196 uL of $MgCl_2$ per 100 mL of actin.

Myosin Preparation from Rabbit:

Rabbits were sacrificed in accordance with NIH guidelines and approved by the Institutional Animal Care and Use Committee (IACUC) at the University of Arizona. The psoas and back muscles of the rabbit were dissected

85

and immediately ground up using a cold meat mincer which had been previously rinsed with 0.02 M EDTA. 100 g of white-muscle meat was collected and immediately extracted using Extraction solution (300 mM KCl, 150 mM KH_2PO_4 pH 6.5, 2 mM EGTA, 2 mM ATP, 1 mM DTT, 5 mM $MgCl_2$ and 0.1 mM NaN_3). After stirring for 10 minutes, the extraction was stopped by adding 1200 mL of cold ddH_2O with 1 mM DTT. The solution was vigorously stirred for a few minutes, and then filtered through cheesecloth into another large beaker. The remaining meat that is captured by the cheesecloth can be stored at -80 °C and used for actin at a later time. 1800 ml of ddH_2O with 1 mM BME was then added slowly into the myosin mixture that went through the cheesecloth with stirring. The combined volume was then stored at 4 °C for about 6-8 hours until the myosin precipitates and settles. The supernatant was decanted off, and the remaining solution with precipitate was centrifuged at 6000 rpm in the JA-10 rotor. The resultant pellet from centrifugation was then dissolved in a minimal volume of 2 M KCl, typically 30 ml. The KCl-myosin mixture was homogenized to get it into solution. The mixture is then dialyzed against myosin dilution solution (600 mM KCl, 25 mM potassium phosphate, 10 mM EDTA, 1 mM DTT, pH 6.5). The goal is to get the myosin and actomyosin to both go into solution.

The next day, the myosin was recovered from the dialysis bag and an equivalent volume of cold ddH_2O is added to the protein. This causes the

actomyosin to precipitate, but not the myosin. The mixture was stirred for 30 minutes on ice. Next, the myosin mixture was centrifuged for 40 minutes at 17,000 rpm in the JA-17 rotor. The supernatant from this centrifugation step was poured over glass wool in a funnel to remove phospholipids from the solution. The resultant myosin solution was then combined with 7 volumes of overnight solution (1 mM DTT, 2 mM $MgCl_2$, 2 mM Potassium Phosphate, pH 7.0). and allowed to stand for several hours. This resulted in the myosin precipitating from the solution.

On the final day of the prep, the precipitated myosin was centrifuged at 6000 rpm for 40 minutes using the JA-10 rotor. The precipitate was then dissolved in high-salt clarification solution (500 mM KCl, 50 mM potassium phosphate, 2 mM $MgCl_2$, 2 mM EGTA, 1 mM DTT, 0.5 mM NaN_3). The solution was then homogenized, and allowed to go into solution. If necessary the myosin can be further clarified by centrifugation at 200,000 xg in an ultracentrifuge, to remove remaining phospholipids. The myosin was then diluted 50x and concentration is measured via UV-spectroscopy. The extinction coefficient for myosin is 0.52. The myosin solution is then diluted to 50% by adding glycerol to the solution. This glycerol-myosin mixture nutated overnight in the cold room, and was then stored at -20 °C. This preparation was performed by Dr. Mark T. McConnell and Sarah J. Lehman, previous graduate students in the Tardiff laboratory.

HMM Preparation from myosin:

2 mL of myosin-glycerol solution was taken from storage at -80 °C and diluted 10x with dilution solution (2 mM MOPS, 2 mM $MgCl_2$, 2 mM DTT). The solution was gently mixed and allowed to rest for 30 minutes on ice. The myosin mixture was then centrifuged at 17,000 RPM for 20 minutes in the JA-17 rotor at 4°C. The resultant pellet was then suspended in 1 mL of high salt solution while still in the centrifuge tube (600 mM KCl, 20 mM KH_2PO_4, 2 mM $MgCl_2$, 2 mM EGTA, 0.1 mM NaN_3, 5 mM DTT, pH 7.0). A flea stir bar was added to the mixture to help suspend the pellet. The centrifuge tube was placed in a room-temperature water bath on the stir plate and 50 uL of 1 mg/mL chymotrypsin suspended in 1 mM HCl was added to the myosin solution and allowed to digest for 10 minutes at room temperature with gentle stirring. To stop digesting, 9 mL of stop solution was added to the mixture (2 mM $MgCl_2$, 2 mM DTT, 1 mM PMSF). The myosin was then allowed to site for at least 30 minutes on ice. The solution was then centrifuged for 15 minutes at 17,000 rpm in the JA-17 rotor. The supernatant was collected and the absorbance was taken via UV-spectroscopy at 280nm, and an extinction coefficient of 0.61. SDS-PAGE was used to confirm complete digestion and purity.

Protein Reconstitution:

The Tn components (cTnT, cTnI, cTnC) were dialyzed individually against a high urea buffer to denature the proteins (6 M urea, 0.5 M KCl, 50 mM MOPS, 1.25 mM $MgCl_2$ 1.25 mM $CaCl_2$, 1.5 mM DTT, pH 7.0.). The concentrations of the proteins were determined via UV spectroscopy. The extinction coefficients were 16960 $M^{-1}cm^{-1}$ at 280 nm for adult cTnT, 4470 $M^{-1}cm^{-1}$ at 280 nm for cTnC, and 9970 $M^{-1}cm^{-1}$ at 280 nm for cTnI. The proteins were combined in a 1.0: 1.2 : 1.2 ratio of cTnT : cTnI : cTnC and placed together into one dialysis bag. The urea was then decreased in a stepwise manner, from 6, to 4, 2, and then 0 M urea, with one step every 6-8 hours, and the rest of the solution constituents remaining constant. Once in 0 M urea solution, the Tn complex was then dialyzed in 0.4 M KCl solution (0.4 M KCl, 50 mM MOPS, 1.25 mM $MgCl_2$ 1.25 mM $CaCl_2$, 1.5 mM DTT, pH 7.0.). TPM and Actin were dialyzed into the same solution, and concentrations were determined via UV spectroscopy. The extinction coefficients were 17880 $M^{-1}cm^{-1}$ at 280 nm for dimeric TPM and 26600 $M^{-1}cm^{-1}$ at 290 nm for actin. Thin filaments could then be dialyzed against appropriate working buffers. Fully reconstituted thin filaments were combined 15 minutes before desired use in 5:5:7 (TPM, Tn, and actin respectively). Total protein concentrations were 1.3mg/mL – 2 mg/mL.

Circular Dichroism

Far-UV circular dichroism (CD) spectra of WT and D230N-TPM were obtained using an Olis DSM-20 (Analytical Biophysics Core, University of Arizona) scanning from 200-260 nm at 20°C. Additionally, the temperature dependence of mean residual ellipticity at 222 nm was monitored from 10°C to 70°C at a heating rate of 2°C·min^{-1} with a 2-minute equilibration period. Far-UV CD spectra were reported at every temperature as an average of ten scans. The samples contained ~0.3 mg/ml of WT or D230N as-TPM in 50 mM sodium phosphate, pH 7.0, 100 mM NaCl, 1 mM $MgCl_2$, and 1 mM βME. Spectra were confirmed through second heating after samples were cooled back down to 10°C suggesting the presence of thermodynamic equilibrium. Mean residual ellipticity was plotted as a function of temperature and the curves were fit in GraphPad via a non-linear least squares fit and EC50 was calculated [44]. . Extra sum of squares F test and least squares fit analysis were used for statistical comparison of WT to D230N-TPM, $p < 0.0001$. Data collected using this technique was performed by Melissa Lynn, a graduate student in the Tardiff Laboratory.

Differential Scanning Calorimetry

For experiments with TPM alone, WT and mutants were dialyzed in a degassed Hepes Buffered Saline (HBS) containing 20 mM MOPS, 0.1 M NaCl,

1 mM EDTA, and 1 mM ß-ME, pH 7.0 [21]. The concentrations of samples were: WT-TPM 1.81 mg/mL and D230N-TPM 1.86 mg/mL. Samples were degassed for 5-10 minutes at 10°C prior to loading into the instrument. A NanoDSC (TA Instruments) was used to assay the thermal stability of the proteins. For each test, equivalent volumes of buffer and sample were loaded. The instrument scanned from 25 to 75 °C at 1.0 °C/min with a 600 second equilibration. A buffer-buffer scan was also performed and applied as the background. Reversibility was checked by scanning each sample twice, during initial and second heating. All of the data was evaluated with the NanoAnalyze DSC Software package. Due to reversibility of the transitions, the data was fitted with a double Gaussian model. The main output for this model is melt temperature (thermal transition, T_m °C), and Enthalpy (ΔH, J/g). The instrument was cleaned between each run with 4% Hellmenex solution, rinsed with 500mL of DI water, and dried prior to loading.

For subsequent experiments containing partially and fully reconstituted thin filaments the troponin complex was reconstituted following the previously described reconstituting protocol, and stepwise urea removal was performed. TPM, Tn complex, and Actin were dialyzed in the HEPES DSC Buffer 3x for at least 4 hours each (HEPES-KOH pH 7.4, 150 mM KCl, 1 mM BME. After 3 changes in dialysis buffer proteins were reconstituted in a 5:5:7 TPM:Tn:Actin ratio (fully reconstituted system) and vacuum degassed prior to loading. The

instrument had been previously cleaned with 1M NaOH for 10min at 90 °C, and confirmed clean by a baseline buffer, buffer run. The reference cell was loaded with Hepes DSC buffer, and the sample cells loaded with the thin filament. The concentration of fully reconstituted samples was kept between 1.3-2.0 mg/mL which is lower due to cTnT's concentration being a limiting factor that changes with each purification. The instrument scanned from 25 °C to 75 °C at 0.5 °C/min with a 600 second equilibration. A buffer-buffer scan was taken and applied as the background for each scan. The data were fitted using the NanoAnalyze software from the instrument manufacturer (TA instruments). For the fully reconstituted thin filaments, a four Gaussian model was sufficient to fit the data. The main output for this model is thermal transition (calorimetric domain, T_m), and Full-width half-max (FWHM). Statistical analysis was performed on all mutants compared to WT using one-way ANOVA.

ATPase protocol and Calcium Sensitivity

The ATPase protocol couples the ATPase activity of cut myosin (HMM) and thin filament proteins in a solution to the absorbance of NADH at 340 nm in a UV spectrophotometer over time. This protocol has been adapted from another group that uses the procedure to test reconstituted thin filaments for functionality [45,46]. The thin filament proteins were reconstituted in the

ratio 4 um actin, 0.8 um Tn, 0.7 um TPM, and 1 um HMM in ATPase solution 10 mM KCl, 4 mM $MgCl_2$, 20 mM Tris-HCl, pH 7.6. To the mixture of proteins, we added to a final concentration of 2 mM phosphoenolpyruvate, 0.3 mM NADH, 38 U/mL of pyruvate kinase, and 50 U/mL of lactate dehydrogenase. The reaction is started upon addition of 2 mM MgATP to the solution. The absorbance at 340 nm was tracked over 20 minutes via UV spectrophotometer, with decreasing absorbance over time due to the conversion of NADH to NAD^+. The assay measures the rate of NADH absorbance decrease at 340nm, which is proportional to the rate of ATP hydrolysis and thus, correlated to the amount of actin-myosin cross bridge formation. The $-Ca^{2+}$ (pCa=9) and $+Ca^{2+}$ (pCa=4.3) states for all mutants were normalized to WT values (Table 4). Calcium Sensitivity was calculated using the equation below:

$$Ca^{2+} \text{ sensitivity} = (ATPase_{-Ca} / ATPase_{+Ca})$$

Statistical Analysis

All values are reported as mean ± S.E.M. calculated using GraphPad Prism5 (San Diego, CA). Statistical analyses including Student's t-test and one-way ANOVA were performed. A p-value of less than 0.05 was accepted as statistically significant.

Molecular Dynamics:

MD simulations were performed by our collaborators in the Schwartz Laboratory, University of Arizona. Molecular modeling of the explicitly solvated fully atomistic thin filament were performed according to published methods [16]. As we have described, a full model of the entire thin filament is necessary to obtain biologically relevant computational predictions, especially when the questions of interest involve the relative placement of one component of the thin filament (TPM) with respect to another (hcTnT). To briefly summarize, the model was generated using NAMD 2.9 using CHARMM27 force field parameters. The models were minimized for 5000 steps. The cell size of the original box was maintained, with periodic boundaries. The particle mesh Ewald (PME) method was used to calculate long range electrostatic interactions and the Van der Waals interactions were cut off at 12 Å. The PME grid spacing was 1.0 Å, and the tolerance was 10^{-6}. The SHAKE algorithm constrained hydrogen length with a tolerance of 1.0^{-8} Å.

The models were heated at a rate of 1 K/ps to 300 K, followed by 10 ps with rescaling at 300 K to ensure the model reached 300 K. The model was then equilibrated for 690 ps in an isothermal-isobaric ensemble, with a Langevin piston used to maintain constant pressure at 1 atm, and a Langevin temperature control maintaining a constant temperature of 300 K. MD production runs of 10 ns were simulated under isothermal-isobaric conditions.

The average structures of the MD production runs allow for the visualization of conformational trends of the models. The resultant fully solvated model contains roughly 5 million atoms and is simulated on the University of Arizona high performance computing facility utilizing GPU equipped nodes.

Snapshots were generated from VMD (Visual Molecular Dynamics) 1.93 software. Standard RMSF VMD plugin was used to generate RMSF plots for each separate trajectory. Then arithmetic average values (from 3 trajectories) were calculated for each residue for WT and D230N. Histograms use a function for finding center of mass, implemented in VMD, then the distances between these points (in cTnT and TM) are measured for each snapshot in trajectory. The number of representatives in each bin was counted using a range of distances from 14 Å to 30 Å with steps 0.5 Å.

References

1. Report of the WHO/ISFC task force on the definition and classification of cardiomyopathies. Br Heart J, 1980. 44(6): p. 672-3.
2. Maron, B.J. et al., Contemporary definitions and classification of the cardiomyopathies: an American Heart Association Scientific Statement from the Council on Clinical Cardiology, Heart Failure and Transplantation Committee; Quality of Care and Outcomes Research and Functional Genomics and Translational Biology Interdisciplinary Working Groups; and Council on Epidemiology and Prevention. Circulation, 2006. 113(14): p. 1807-16.
3. van de Meerakker, J. B. et. al., *A novel alpha tropomyosin mutation associates with dilated and non-compaction cardiomyopathy and diminishes actin binding*. Biochimica et Biophysica Acta, 2013. p. 833-839.
4. Spudich, J.A., Hypertrophic and Dilated Cardiomyopathy: Four Decades of Basic Research on Muscle Lead to Potential Therapeutic Approaches to These Devastating Genetic Diseases. Biophysical Journal, 2014. 106: p. 1236-1249.
5. Teare, D. et al., Asymmetrical Hypertrophy of the Heart in Young Adults. British Heart Journal, 1958. 20: p. 1-8.
6. Gordon, A. M., Homsher, E., and Regnier, M. Regulation of contraction in striated muscle. Physiological reviews, 2000. 80: p. 853-924.
7. Ruppel, K. M., and Spudich, J. A. Structure-function analysis of the motor domain of myosin. Annual review of cell and developmental biology, 1996. 12: p. 543-573.
8. Egelman, E. H., The structure of F-actin. Journal of muscle research and cell motility, 1985. 6: p. 129-151
9. Greaser, M. L., and Gergely, J. (1973) Purification and Properties of the Components from Troponin. *Journal of Biological Chemistry* **248**, 2125-2133
10. Cooper GM. The Cell: A Molecular Approach. 2nd edition. Sunderland (MA): Sinauer Associates; 2000. Actin, Myosin, and Cell Movement. Available from: https://www.ncbi.nlm.nih.gov/books/NBK9961/
11. Lupas, A. N., and Gruber, M. (2005) The structure of alpha-helical coiled coils. Advances in protein chemistry 70, 37-78
12. Morimoto, S. (2008) Sarcomeric proteins and inherited cardiomyopathies. Cardiovasc Res 77, 659-666
13. Poole, K. J., Lorenz, M., Evans, G., Rosenbaum, G., Pirani, A., Craig, R., Tobacman, L. S., Lehman, W., and Holmes, K. C. (2006) A comparison of

muscle thin filament models obtained from electron microscopy reconstructions and low-angle X-ray fibre diagrams from non-overlap muscle. *Journal of structural biology* **155**, 273-284

14. Holmes, K. C., and Lehman, W. (2008) Gestalt-binding of tropomyosin to actin filaments. *Journal of muscle research and cell motility* **29**, 213-219

15. Palm, T., Graboski, S., Hitchcock-DeGregori, S. E., and Greenfield, N. J. (2001) Disease-Causing Mutations in Cardiac Troponin T: Identification of a Critical Tropomyosin-Binding Region. *Biophysical Journal* **81**, 2827-2837

16. Palm, T., Greenfield, N. J., and Hitchcock-DeGregori, S. E. (2003) Tropomyosin Ends Determine the Stability and Functionality of Overlap and Troponin T Complexes. *Biophysical Journal* **84**, 3181-3189

17. Barua, B. (2013) Periodicities designed in the tropomyosin sequence and structure define its functions. *Bioarchitecture* **3**, 51-56

18. Williams, M.R., et al., *Atomic resolution probe for allostery in the regulatory thin filament.* Proc Natl Acad Sci U S A, 2016. **113**(12): p. 3257-62.

19. Nitanai, Y., et al., *Crystal structures of tropomyosin: flexible coiled-coil.* Adv Exp Med Biol, 2007. **592**: p. 137-151.

20. Holmes, K. and W. Lehman, *Gestalt-binding of tropomyosin to actin filaments.* J Muscle Res Cell Motil, 2008. **29**: p. 213-219.

21. Yar, S., et al., *Conserved Asp-137 is important for both structure and regulatory functions of cardiac □-tropomyosin (□-TM) in a novel transgenic mouse model expressing Alpha-TM-D137L.* J Biol Chem, 2013. **288**(23): p. 16235-46.

22. Gordon, A., M. Regnier, and E. Homsher, *Skeletal and cardiac muscle contraction activation: Tropomyosin "rocks and rolls".* News Physiol Sci, 2001. **16**(2): p. 49-55.

23. Boussouf, S. and M. Geeves, *Tropomyosin and troponin cooperativity on the thin filament.* Adv Exp Med Biol, 2007. **592**: p. 99-109.

24. McKillop, D. and M. Geeves, *Regulation of the interaction between actin and myosin subfragment 1: Evidence for three states of the thin filament.* Biophysical Journal, 1993. **65**: p. 693-701.

25. Geisterfer-Lowrance, A.A., et al., *A molecular basis for familial hypertrophic cardiomyopathy: a beta cardiac myosin heavy chain gene missense mutation.* Cell, 1990. **62**(5): p. 999-1006.

26. Lakdawala, N., et al., *Familial dilated cardiomyopathy caused by an alpha-tropomyosin mutation: The distinctive natural history of sarcomeric dilated cardiomyopathy.* J Am Coll Cardiol, 2010. **55**: p. 320-329.

27. Jongbloed, R.J., et al., *Variable Clinical Manifestation of a Novel Missense Mutation in the Alpha-Tropomyosin (TPM1) Gene in Familial Hypertrophic Cardiomyopathy.* JACC, 2003. 41(6): p. 981-986.

28. Nirody, J., et al., *Electron microscopy and molecular dynamics on a D137L mutant of tropomyosin.* 2010.

29. Tardiff, J., *Thin filament mutations: Developing an integrative approach to a complex disorder.* Circ Research, 2011. **108**: p. 765-782.

30. Matyushenko, A., et al., *effects of two stabilizing mutations, D137L and G126R, in the middle part of ☐☐tropomyosin on the domain structure of its molecule.* Biophys Chem, 2015. **196**: p. 77-85.

31. Bruylants, G, et al., *Differential Scanning Calorimetry in Life Science: Thermodynamics, Stability, Molecular Recognition and Application in Drug Design.* Medicinal Chemistry, 2005. 12: p. 2011-2020.

32. Kremneva, E.V., Nikolaeva, O.P., Gusev, N.B., Levitsky, D.I., *Effects of Troponin on Thermal Unfolding of Actin-Bound Tropomyosin.* Biochemistry (Moscow), 2003. 68(7): p. 976-984.

33. Schober, T., et al., *Myofilament ca sensitization increases cytosolic ca binding affinity, alters intracellular ca homeostasis, and causes pause-dependent ca-triggered arrhythmia.* . Circulation Research, 2012. **111**: p. 170-179.

34. Phillips, G., Jr, J. Fillers, and C. Cohen, *Tropomyosin crystal structure and muscle regulation.* J Mol Biol, 1986. **192**: p. 111-131.

35. Singh, A. and S. Hitchcock-DeGregori, *Local destabalization of the tropomyosin coiled coil gives the molecular flexibility required for actin binding.* Biochemistry, 2003. **42**: p. 14114-14121.

36. Singh, A. and S. Hitchcock-DeGregori, *Dual requirement for flexibility and specificity for bidning of the coiled-coil tropomyosin to its target, actin* Structure, 2006. **14**: p. 43-50.

37. Brown, J.H., Cohen, C., *Regulation of Muscle Contraction by Tropomyosin and Troponin: How Structure Illuminates Function.* Advances in Protein Chemistry, 2005. 71: p. 121-159

38. Sousa, D. R., Stagg, S. M., and Stroupe, M. E. (2013) CRYO-EM STRUCTURES OF THE ACTIN: TROPOMYOSIN FILAMENT REVEAL THE MECHANISM FOR THE TRANSITION FROM C- TO M-STATE. *Journal of molecular biology* **425**, 10.1016/j.jmb.2013.1008.1020

39. von der Ecken, J., Muller, M., Lehman, W., Manstein, D. J., Penczek, P. A., and Raunser, S. (2015) Structure of the F-actin-tropomyosin complex. *Nature* **519**, 114-117

40. Singh, A., Hitchcock-DeGregori, S.E., *A Peek into Tropomyosin Binding and Unfolding Actin Filament.* PLoS ONE, 2009. 4(7): e6336.

41. Hitchcock-DeGregori, S. E., and Heald, R. W. (1987) Altered actin and troponin binding of amino-terminal variants of chicken striated muscle alpha-tropomyosin expressed in Escherichia coli. *The Journal of biological chemistry***262**, 9730-9735

42. Matyushenko, A.M., et al., *Structural and Functional Effects of Cardiomyopathy-Causing Mutations in the Troponin T-Binding Region of Cardiac Tropomyosin.* Biochemistry, 2017. **56**(1): p. 250-259.

43. Wnendt, S. (1994) Analysis of the endA mutation of Escherichia coli K12 strains: JM103 behaves like endA+ wild-type strains. *BioTechniques* **17**, 270, 272

44. Greenfield, N., *Using circular dichroism collected as a function of temperature to determine the thermodynamics of protein unfolding and binding interactions.* Nat Protoc, 2006. **1**(6): p. 2527-2535.

45. Ueda, K., Kimura-Sakiyama, C., Aihara, T., Miki, M., and Arata, T. Interaction Sites of Tropomyosin in Muscle Thin Filament as Identified by Site-Directed Spin-Labeling. *Biophysical Journal* **100**, 2432-2439

46. Matsuo, N., Nagata, Y., Nakamura, J., and Yamamoto, T. (2002) Coupling of calcium transport with ATP hydrolysis in scallop sarcoplasmic reticulum. *Journal of biochemistry* **131**, 375-381

47. Hwang, T.J., et al., *Temporal Trends and Factors Associated With Cardiovascular Drug Development, 1990 to 2012.* JACC: Basic to Translational Science, 2016. **1**(5): p. 301.